The Astrophysical Journal, 643:863–880, 2006 June 1

TYPE Ia SUPERNOVAE IN A HIERARCHICAL GALAXY FORMATION MODEL: THE MILKY WAY

Masahiro Nagashima[1,2] and Takashi Okamoto[1,3]
Received 2004 December 7; accepted 2006 February 2

ABSTRACT

We investigate chemical evolution in Milky Way–like galaxies based on the cold dark matter model in which cosmic structures form via hierarchical merging. We introduce chemical enrichment due to Type Ia supernovae (SNe Ia) into the Mitaka semianalytic galaxy formation model developed by Nagashima & Yoshii. For the first time we derive distributions of stellar metallicities and their ratios in Milky Way–like galaxies treating chemical enrichment due to SNe Ia in a hierarchical galaxy formation model self-consistently. As a first attempt, we assume all SNe Ia to have the same lifetime and assume instantaneous recycling for Type II supernovae (SNe II). We find that our model reproduces well the metal abundance ratio [O/Fe] against [Fe/H] and the iron metallicity distribution function in the solar neighborhood. This means that the so-called G dwarf problem is resolved by the hierarchical formation of galaxies, and a gas infall term introduced in traditional monolithic collapse models to solve this problem is well explained by the mixture of some physical processes such as hierarchical merging of dark halos, gas cooling, energy feedback, and injection of gas and metals into hot gas due to supernovae. We also discuss how physical processes affect the metal abundance ratio by varying the lifetime of SNe Ia, the star formation timescale, and the strength of supernova feedback. We find that the supernova feedback plays a key role among them, and therefore there is no one-to-one correspondence between star formation histories and stellar metallicity ratio distributions.

Subject headings: Galaxy: abundances — Galaxy: evolution — Galaxy: formation — large-scale structure of universe — stars: abundances

Online material: color figures

1. INTRODUCTION

The chemical compositions of stars and gas, as is widely known, provide important clues to understanding the formation and evolution of galaxies. In particular, the abundance ratio of α-elements such as oxygen to iron is a useful probe of the formation history of galaxies. The main sources of metals are considered to be supernovae (SNe), especially Type II SNe (SNe II) and Type Ia SNe (SNe Ia). They have different abundance patterns; the former produces α-elements as well as iron, and the latter produces hardly any α-elements. Therefore, the measurement of [α/Fe] is closely related to the ratio of SNe II to SNe Ia. While the progenitors of SNe II are massive stars larger than $\sim$10 $M_{\odot}$, those of SNe Ia are considered to be white dwarfs in binary systems. Therefore, the explosion rate of SNe II is almost proportional to the star formation rate of their progenitor stars at that time, but there is a time lag between SNe Ia explosions and the formation of their progenitor stars. Since the evolution timescales of those elements are independent and different, we can obtain useful information on galaxy formation and star formation histories from the abundance ratio of those elements.

Because SNe II explode almost instantaneously, the chemical evolution process has usually been formulated by assuming that massive stars immediately explode right after their formation (the instantaneous recycling [IR] approximation; Tinsley 1980; Lacey & Fall 1983, 1985). In those works, galaxies are usually assumed to grow up in monolithic clouds, in which timescales of gas infall and star formation (SF) are typically treated as free parameters. Since it is possible to observe and resolve individual stars in the solar neighborhood, many studies have focused on evolution of the galactic disk. By adjusting those parameters and by incorporating stellar population synthesis techniques (Arimoto & Yoshii 1986, 1987), detailed galaxy evolution models that reproduce observations have been developed (Arimoto et al. 1992).

In the framework of such traditional galaxy evolution models, several authors explicitly considered chemical enrichment due to SNe Ia (Greggio & Renzini 1983; Matteucci & Greggio 1986; Matteucci & François 1989; Tsujimoto et al. 1995; Pagel & Tautvaišienė 1995; Yoshii et al. 1996). They included delayed production of metals due to SNe Ia in the galaxy evolution models. By comparing their models with solar neighborhood stars in the metallicity distribution function (MDF) and abundance ratios such as [O/Fe] against metallicity, Pagel & Tautvaišienė (1995) and Yoshii et al. (1996) inferred a typical lifetime of SNe Ia of $\sim$1.3–1.5 Gyr. Although Kobayashi et al. (1998) have claimed that SNe Ia start to explode at the age of about 0.6 Gyr, Gal-Yam & Maoz (2004) recently derived that the lifetime should be longer than about 1 Gyr at the 99% confidence level by comparing the cosmic star formation history with the cosmic SN Ia rate.

Considered from the viewpoint of cosmological structure formation, however, these models are still only phenomenological. Recent theoretical and observational studies of structure formation have revealed that the universe is dominated in mass by cold dark matter (CDM) and that baryonic objects such as galaxies form in virialized objects of dark matter called dark halos. In the CDM model, since smaller scale density fluctuations in the early universe have larger fluctuation amplitudes, larger halos form through mergers of smaller dark halos (the hierarchical clustering scenario). This suggests that large galactic gas clouds would have formed at low redshift by mergers of

[1] Department of Physics, University of Durham, South Road, Durham DH1 3LE, UK.
[2] Department of Physics, Graduate School of Science, Kyoto University, Sakyo-ku, Kyoto 606-8502, Japan; masa@scphys.kyoto-u.ac.jp.
[3] Division of Theoretical Astrophysics, National Astronomical Observatory, National Institute of Natural Science, Mitaka, Tokyo 181-8588, Japan.

subgalactic clumps that have formed at higher redshift. Therefore, we may have to modify our picture of chemical evolution in galaxies as well as that of galaxies themselves.

Recently, based on a semianalytic (SA) approach, galaxy formation models in the hierarchical clustering scenario have been developed in which the formation histories of individual dark halos are followed by using a Monte Carlo method and physical processes such as gas cooling and star formation are taken into account in the histories of dark halos. This is a natural consequence of adopting the CDM model, because we are not able to freely assume formation histories of dark halos as far as we would like to construct galaxy formation models consistent with the CDM model. Many authors have found that such SA models reproduce well various characteristics of galaxies at the present and at high redshift, such as luminosity functions, gas fractions, size distributions, and faint galaxy number counts (e.g., Kauffmann et al. 1993; Cole et al. 1994, 2000; Nagashima et al. 1999, 2001, 2002; Nagashima & Yoshii 2004; Somerville & Primack 1999; Somerville et al. 2001). In recent SA models, chemical enrichment is considered, but generally only with the IR approximation. Kauffmann & Charlot (1998) and Nagashima & Gouda (2001) investigated color-magnitude and metallicity-magnitude relations of cluster elliptical galaxies. This is extended to dwarf spheroidals, $M_B \sim -10$, by Nagashima & Yoshii (2004). Kauffmann (1996), Somerville et al. (2001), and Okoshi et al. (2004) consider chemical evolution in spiral galaxies, some of which should be identified as damped Lyα systems. Some of them found good agreement with observations.

Pioneering work taking into account chemical enrichment due to SNe Ia in a SA model was carried out by Thomas (1999) and Thomas & Kauffmann (1999). In those papers, they picked out averaged and individual formation histories of dark halos, and then, assuming the closed-box chemical evolution, they followed star formation and chemical enrichment histories. Thus, while they took into account merging histories of galaxies, the outflow of gas caused by SNe or the SN feedback that has been realized to be a primarily important process in galaxy formation was not considered. As shown by Kauffmann & Charlot (1998) and Nagashima & Gouda (2001), SN feedback significantly affects chemical enrichment, at least due to SNe II. This suggests that the closed-box model has limitations in analyzing chemical evolution in a realistic situation.

As a complementary approach to SA modeling, chemodynamical simulations including SNe Ia have been developed (e.g., Raiteri et al. 1996; Berczik 1999; Kawata 2001; Lia et al. 2002; Nakasato & Nomoto 2003; Kobayashi 2004; Okamoto et al. 2005). Although this approach has an advantage in resolving spatial structure, because of the limitation of numerical resolution and numerical techniques themselves, further improvements are still required (Okamoto et al. 2003). On the other hand, the SA model is free from numerical effects and limitations. This is a great advantage for understanding global properties of galaxy formation, because in principle the SA model can investigate from dwarf galaxies to galaxy clusters simultaneously.

In this paper we construct a fully self-consistent treatment of chemical enrichment with a SA model. The basic model is the Mitaka model presented by Nagashima & Yoshii (2004), which includes a Monte Carlo realization of the merging histories of dark halos, radiative gas cooling, quiescent star formation and starbursts, mergers of galaxies, chemical enrichment assuming the IR approximation, size estimation of galaxies taking into account the dynamical response to gas removal during starbursts, and stellar population synthesis. As a first attempt, we assume that all SNe Ia have the same lifetime. This is, of course, a rather simplified model. In reality the lifetimes of SNe Ia are considered to have a broad distribution, and there is even a claim that low-metallicity environments inhibit SNe Ia (Kobayashi et al. 1998). Our model, however, has an essential characteristic of SNe Ia, that is, the time lag between star formation and the explosion. It enables us to see how such a delayed explosion of SNe Ia affects the chemical enrichment and abundance pattern in galaxies. Using this model, we focus on the chemical enrichment in Milky Way (MW)-like galaxies. This has a particular meaning, because there are many nontrivial effects on the chemical enrichment in the hierarchical formation of galaxies. Massive galaxies such as the MW form not only via gas cooling but via mergers of pregalactic subclumps with stronger efficiencies of the SN feedback than those in massive galaxies residing in deeper gravitational potential wells. Thus, the main purpose of this paper is to compare the SA model with a monolithic collapse model of Yoshii et al. (1996). This enables us to see how the hierarchical formation process affects galactic metal enrichment due to SNe Ia based on the CDM model. Further comparison to other objects will be done in subsequent papers.

This paper is outlined as follows. In § 2 we describe our SA model. In § 3 we provide a detailed prescription of the chemical enrichment due to SNe Ia. In § 4 we show the luminosity function of galaxies that should be compared with that in the Local Group and properties of MW-like galaxies. In § 5 we compare our model with observations in the [O/Fe]-[Fe/H] plane and the [Fe/H] distribution in a statistical sense. In § 6 we briefly discuss individual galaxies. In § 7 we investigate parameter dependences of the main results. In § 8 we provide a summary and conclusions.

2. SEMIANALYTIC MODEL

Here we briefly describe how to form galaxies in our model, which is based on the Mitaka model (Nagashima & Yoshii 2004). In a CDM universe, dark matter halos cluster gravitationally and grow in mass through their mergers, depending on the adopted power spectrum of the initial density fluctuations. In each of the merged dark halos, radiative gas cooling, star formation, and gas reheating by supernovae occur. The cooled dense gas and stars constitute *galaxies*. These galaxies sometimes merge together in a common dark halo, and then more massive galaxies form. During these processes, chemical enrichment due to SNe II is solved by assuming the IR approximation, and the enrichment due to SNe Ia, by using the past star formation histories of individual galaxies (see § 3). Repeating these processes, galaxies form and evolve to the present epoch. The Mitaka model reproduces many observations, such as luminosity functions, the cold gas fraction, sizes of disks and spheroidals, surface brightnesses, the Faber-Jackson relation, the mass-to-light ratio, and faint galaxy number counts. The details, apart from chemical enrichment due to SNe Ia, are found in Nagashima & Yoshii (2004).

Throughout this paper, we consider only a Λ-dominated CDM (ΛCDM) cosmology with $\Omega_0 = 0.3$, $\Omega_\Lambda = 0.7$, $h = 0.7$, $\sigma_8 = 0.9$, and $\Omega_b = 0.02\ h^{-2}$ and a power spectrum given by Sugiyama (1995), which takes into account the effects of baryons.

The merging histories of dark halos are calculated by using a method given by Somerville & Kolatt (1999). The time step is $\Delta z = 0.06(1 + z)$, which corresponds to the dynamical timescale of dark halos collapsing at z. Only dark halos with circular velocities larger than $V_{\rm low} = 40$ km s^{-1} are regarded as isolated halos. While the value of $V_{\rm low}$ hardly affects the chemical evolution in the MW-like galaxies that we consider in this paper, we compare the luminosity function of galaxies in the Local Group

(LG) with the model luminosity functions with various $V_{\rm low}$ in § 4. The circular velocities of *root* halos, which are halos at $z = 0$, are set to be $V_{\rm circ} = 220$ km s^{-1}, which is nearly equal to the rotation speed of the MW.

The cycle among baryonic components in dark halos is computed as follows. Diffuse baryonic gas is shock heated to the virial temperature estimated from the depth of the gravitational potential well of its host dark halo when it collapses. This is called hot gas, whose mass is $M_{\rm hot}$. The hot gas dissipates its energy and cools by radiation only for halos with $V_{\rm circ} \le V_{\rm cut} = 250$ km s^{-1}, to avoid formation of unphysically giant galaxies, in each time step. The cooling rate is estimated by using the metallicity-dependent cooling functions given by Sutherland & Dopita (1993). This cooled gas concentrates in the vicinity of the center of the dark halo and constitutes a galactic disk. The mass of cold gas is $M_{\rm cold}$. Disk stars form by consuming the cold gas with a star formation timescale τ_*. In proportion to the star formation rate $\psi = M_{\rm cold}/\tau_*$, massive stars explode as SNe II. The energy released by SNe II reheats the cold gas, and a part of the cold gas is absorbed into the hot gas (SN feedback). The reheating rate is given by $\dot{M}_{\rm reheat} = \beta\psi$, where $\beta = (V_{\rm disk}/V_{\rm hot})^{-\alpha_{\rm hot}}$ and $V_{\rm hot}$ and $\alpha_{\rm hot}$ are free parameters. In this paper the star formation timescale is assumed to be $\tau_*^0(1 + \beta)$, where τ_*^0 is a free parameter, which is called the constant star formation model (CSF) in Nagashima & Yoshii (2004). Because β is much larger than unity in low-mass halos owing to their shallower gravitational potential wells, most cold gas is reheated and only a small fraction of it turns into stars. The above processes are computed during each time step.

When a dark halo collapses by merging two or more dark halos, the hot gas components in the progenitor halos are immediately merged and constitute a hot gas component in the new dark halo. In contrast, galaxies do not merge together immediately. At first we define a central galaxy in the newly collapsing dark halo as the central galaxy in the most massive progenitor halo, and the rest of the galaxies are regarded as satellite galaxies. Two modes of galaxy mergers are considered. One is a merger between central and satellite galaxies, in which a satellite falls into a central galaxy after losing its energy by dynamical friction (Binney & Tremaine 1987). Another is that between satellite galaxies by random collisions (Makino & Hut 1997). We estimate the timescales of the dynamical friction and the random collisions for all satellites. Satellites with sufficiently short merger timescales compared with the timescale of subsequent collapse of the dark halo merge with a central galaxy or other satellite galaxies. If the mass ratio of stars and cold gas of a smaller galaxy to a larger one, $f = m_{\rm small}/m_{\rm large}$, is larger than $f_{\rm bulge}$, a starburst occurs with SN feedback, and all stars go into the bulge component. Then no cold gas remains. Otherwise, the smaller satellite is simply absorbed into the disk component of the central or larger satellite without any activities of star formation. We adopt $f_{\rm bulge} = 0.4$.

In each time step, the disk size is estimated as a rotationally supported disk under the assumption of specific angular momentum conservation for cooling hot gas. Initially, hot gas is assumed to have the same specific angular momentum as that of its host dark halo. The angular momentum of dark halos has a log-normal distribution in terms of the so-called dimensionless spin parameter. If the estimated disk size is larger than before, we renew the size. At the same time, we also set the disk rotation velocity to be the same as $V_{\rm circ}$ of the dark halo. When a major merger occurs, the bulge size is estimated by assuming energy conservation. Then a starburst occurs. Because the mass of the galaxy after the starburst is different from that before, we consider the dynamical response to the mass loss of the size and velocity dispersion. To do this, we use the formalism of the dynamical response taking into account the underlying dark matter potential developed by Nagashima & Yoshii (2003). This process is required to reproduce observed characteristics of dwarf spheroidals, such as surface brightness and velocity dispersion.

Through the above processes, we obtain star formation histories of individual galaxies. From those we estimate the luminosities of galaxies using a stellar population synthesis technique. We adopt the simple stellar populations given by Kodama & Arimoto (1997).

These procedures are the same as those in Nagashima & Yoshii (2004). Readers who are interested in the details will find them in that paper. The key parameters of the model are tabulated in Table 1.

TABLE 1
Model Parameters

$V_{\rm hot}$ (km s^{-1})	$\alpha_{\rm hot}$	τ_*^0 (Gyr)	$y_{\rm II,O}$	$y_{\rm II,Fe}$	$y_{\rm Ia,Fe}$
150.....	4	1.3	7.19×10^{-3}	3.40×10^{-4}	6.67×10^{-4}

Notes.—The $V_{\rm hot}$, $\alpha_{\rm hot}$, and τ_*^0 are determined by matching the luminosity functions of galaxies and the mass fraction of cold gas in spiral galaxies with observations. See Nagashima & Yoshii (2004) for details. The above chemical yields are the same as those adopted by Yoshii et al. (1996). In the case of Salpeter's IMF (Salpeter 1955) with a slope of 1.35, according to their paper, the lower and upper mass limits correspond to 0.03 and 50 $M_\odot$, respectively. The so-called A-parameter determining binary fractions is 0.015–0.055.

3. CHEMICAL ENRICHMENT

The chemical enrichment is treated in a similar manner to that of Yoshii et al. (1996), in which they considered chemical enrichment of oxygen (O) and iron (Fe) due to both SNe II and SNe Ia using the infall model in the framework of monolithic collapse (Arimoto et al. 1992). In their paper, the basic equations describing the gas fraction, f_g, and metallicities for the ith elements, Z_i, are written as

$$\frac{df_g}{dt} = -\alpha\psi(t) + A(t), \tag{1}$$

$$\frac{d(Z_i f_g)}{dt} = -\alpha Z_i(t)\psi(t) + Z_{A,i}A(t) + \alpha y_{{\rm II},i}\psi(t) + \alpha y_{{\rm Ia},i}\int_0^t \psi(t - t_{\rm Ia})g(t_{\rm Ia})\,dt_{\rm Ia}, \tag{2}$$

where $A(t)$ denotes the gas infall rate, $g(t_{\rm Ia})$ is a distribution function of the lifetime of SNe Ia $t_{\rm Ia}$, α is the locked-up mass fraction in low-mass stars and dead stellar remnants, and $y_{{\rm II},i}$ and $y_{{\rm Ia},i}$ are the chemical yields of the ith element produced by SNe II and SNe Ia, respectively (see eqs. [1] and [2] in their paper). The star formation rate ψ is assumed to obey the Schmidt law (Schmidt 1963),

$$\psi(t) = \nu f_g^k, \tag{3}$$

where ν is a rate coefficient. The infall term is assumed to be

$$A(t) = \frac{(t/t_{\rm in})^\gamma \exp(-t/t_{\rm in})}{t_{\rm in}\Gamma(\gamma + 1, T_G/t_{\rm in})}, \tag{4}$$

where $t_{\rm in}$ is the infall timescale, $\Gamma(a, b)$ is the incomplete gamma function, and T_G is the age of the Galaxy. In the following, we compare our results with their $k = 1$ model having $k = 1$, $(\alpha\nu)^{-1} = 3.01$ Gyr, $t_{\rm in} = 5$ Gyr, $\gamma = 1$, and a constant lifetime of SNe Ia $g(t_{\rm Ia}) = \delta^{\rm D}(t_{\rm Ia} - 1.5\ {\rm Gyr})$. This value of the lifetime of SNe Ia is consistent with a theoretically estimated value using a model of Lia et al. (2002), which is based on Greggio & Renzini (1983), assuming Kennicutt's initial mass function (IMF) of stars (Kennicutt 1983). We have estimated that the mean lifetime is about 2.4 Gyr, and the median, about 1.8 Gyr.

In our model, because of the SN feedback, these equations are modified. During disk star formation or a starburst in a time step that corresponds to $\Delta z = 0.06(1 + z)$, chemical enrichment due to SNe II is solved by assuming the IR approximation,

$$\frac{dM_{\rm cold}}{dt} = -(\alpha + \beta)\psi(t), \tag{5}$$

$$\frac{dM_{\rm hot}}{dt} = \beta\psi(t), \tag{6}$$

$$\frac{d(M_{\rm cold}Z_{{\rm cold},i})}{dt} = -(\alpha + \beta)Z_{{\rm cold},i}\psi(t) + \alpha y_{{\rm II},i}\psi, \tag{7}$$

$$\frac{d(M_{\rm hot}Z_{{\rm hot},i})}{dt} = \beta Z_{{\rm cold},i}\psi, \tag{8}$$

where $Z_{{\rm cold},i}$ and $Z_{{\rm hot},i}$ are metallicities for the ith element of cold and hot gas, respectively. The star formation rate ψ is given by $M_{\rm cold}/\tau_*$. Equations (5)–(8) do not have infall terms, because we add the mass of hot gas that should cool during a time step Δz to the mass of cold gas at the beginning of each time step. The time step is sufficiently short to describe smooth gas accretion. Therefore, no infall term is required as an approximation. The mixture of merging histories of dark halos, gas cooling, and SN feedback should correspond to the infall process with a long timescale, $\sim$5 Gyr. The roles of the physical processes are clarified in § 6. In addition to this process, metals released from SNe Ia are put into the cold gas. The mass of ith element released during a time step $[t_{j-1}, t_j]$ is

$$\Delta M_i = \alpha y_{{\rm Ia},i}\int_{t_{j-1}}^{t_j}\psi(t - t_{\rm Ia})\,dt. \tag{9}$$

In order to estimate this quantity, star formation histories of individual galaxies are stored. Again, we would like to stress that the above procedures of chemical enrichment due to both SNe Ia and II are computed in each time step.

Since one of the main purposes of this study is to compare our results with a monolithic cloud model given by Yoshii et al. (1996), we adopt the same chemical yields empirically determined by their analysis, which are also tabulated in Table 1. Thus, we also impose two nucleosynthesis constraints they adopted: $y_{\rm II,O}/y_{\rm II,Fe} = {\rm const}$ and $y_{\rm Ia,O} = 0$. Returned mass from SNe Ia is simply treated together with that from massive stars, that is, it is included in a parameter for the instantaneous recycling, $1 - \alpha$. For simplicity, we do not take into account the following effects that might affect chemical evolution of galaxies. One is energy feedback due to SNe Ia, which was investigated in detail in Kawata & Gibson (2003a, 2003b). Second is inhomogeneous star formation in a gas cloud considering propagation of star formation sites, which is another way to extend the simple traditional galaxy evolution model (Tsujimoto et al. 1999; Ishimaru & Wanajo 1999). Although it will probably provide a broader distribution in metal abundances, we concentrate, in this paper, on how the hierarchical formation process affects the chemical enrichment. Third is the metallicity effect in which a low-metallicity environment inhibits the explosion of SNe Ia (Kobayashi et al. 1998), which might affect the estimation of $t_{\rm Ia}$. These effects would be worth considering in the future.

4. LUMINOSITY FUNCTION AND GLOBAL CHARACTERISTICS OF MW-LIKE GALAXIES

The model we use here is the same as that in Nagashima & Yoshii (2004), except for the chemical enrichment process, which does not affect any results in that paper. Therefore, we do not repeat showing the same figures as shown in that paper.

In the following, we pick out galaxies in dark halos of $V_{\rm circ} = 220$ km s^{-1} whose central galaxies are identified as spiral galaxies with B-band bulge to total luminosity ratios smaller than 0.4 (Baugh et al. 1996) and with $-22.1 \le M_I - 5\log h \le -21.6$ (Somerville & Primack 1999) and disk rotation velocities $210 \le V_{\rm disk}/{\rm km\ s^{-1}} \le 230$ (Benson et al. 2002b). Hereafter, we call a dark halo satisfying the above criteria a LG halo. We realize 100 LG halos and average over the realization.

Before entering the details, we see the characteristics of MW-like galaxies and their satellites. In Figure 1*a* we show a luminosity function of galaxies in LG halos. The solid line indicates the model luminosity function, and the histogram, the observed one compiled by M. Irwin.[4] Because the observed data are for the MW and M31 groups, luminosity functions for models are simply doubled to be compared with the observed data.

Our model shows a broad agreement with the observed luminosity function in the LG at $M_B \lesssim -15$, although at fainter magnitude too many galaxies are predicted. While the observed luminosity functions actually depend on the definition of the Local Group, our conclusion about the chemical evolution of the MW-like galaxies does not change, as shown below. The detailed discussion is given by Benson et al. (2002a).

Such an overabundance of low-luminosity galaxies is easily eliminated by taking into account some physical or observational effects, as shown by many authors. One of the important effects is photoionization due to ultraviolet (UV) background or reionization (e.g., Nagashima et al. 1999; Nagashima & Gouda 2001; Somerville 2002; Benson et al. 2002a, 2002b, 2003). Here we show the effect of the Jeans mass increasing due to reionization in a simple way by changing $V_{\rm low}$. Note that in reality this effect should turn on only after the epoch of reionization. Indeed, this simple model is similar to that in Kauffmann et al. (1993), in which they assumed that gas cooling is prohibited in dark halos with $V_{\rm circ} \le 150$ km s^{-1} at redshifts between 1.5 and 5 to be consistent with the LG luminosity function in the standard CDM model. In Figure 1*b*, we show luminosity functions with different $V_{\rm low}$. As shown in the panel, the solid, dashed, dot-dashed, and dotted lines indicate $V_{\rm low} = 40$ (the reference model), 30, 50, and 70 km s^{-1}, respectively. Evidently, large $V_{\rm low}$ inhibits the formation of dwarf galaxies. Another effect is incompleteness in the observations. Nagashima & Yoshii (2004) predict that there are many dwarf galaxies with surface brightnesses too low to detect. In the bottom panel, Figure 1*c*, we show luminosity functions with different threshold surface brightnesses $S_{\rm th}$, which determines the lowest surface brightness of galaxies to be detected. The solid, dashed, dot-dashed, and dotted lines indicate $S_{\rm th} = \infty$, 26, 25, and 24 mag arcsec^{-2}, respectively, where

[4] See http://www.ast.cam.ac.uk/~mike/local_members.html.

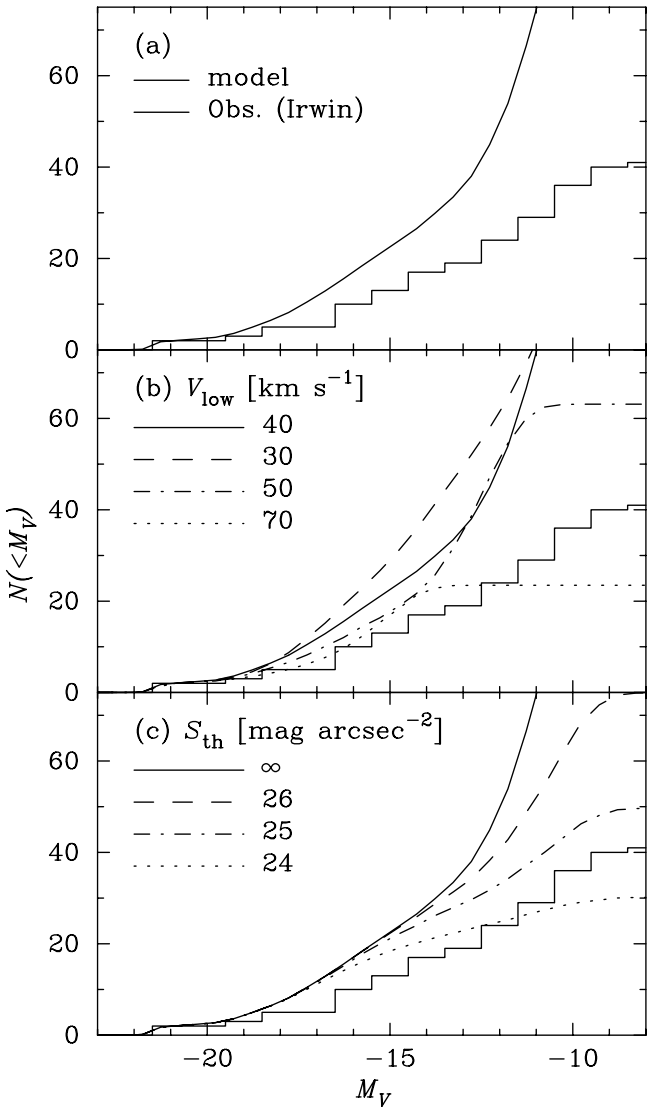

FIG. 1.—Cumulative luminosity function in the LG. (*a*) The solid line indicates the reference model. The histogram denotes the observed luminosity function in the LG compiled by M. Irwin. (*b*) Dependence on V_{low}. The solid line is the same as the model in (*a*), the reference model of $V_{low} = 40$ km s^{-1}. The dashed, dot-dashed, and dotted lines indicate variants of the reference model with $V_{low} = 30$, 50, and 70 km s^{-1}. (*c*) Dependence on S_{th}. The solid line is the same as the model in (*a*), the reference model of $S_{th} = \infty$. The dashed, dot-dashed, and dotted lines indicate variants of the reference model with $S_{th} = 26$, 25, and 24 mag arcsec^{-2}, respectively. [*See the electronic edition of the Journal for a color version of this figure*.]

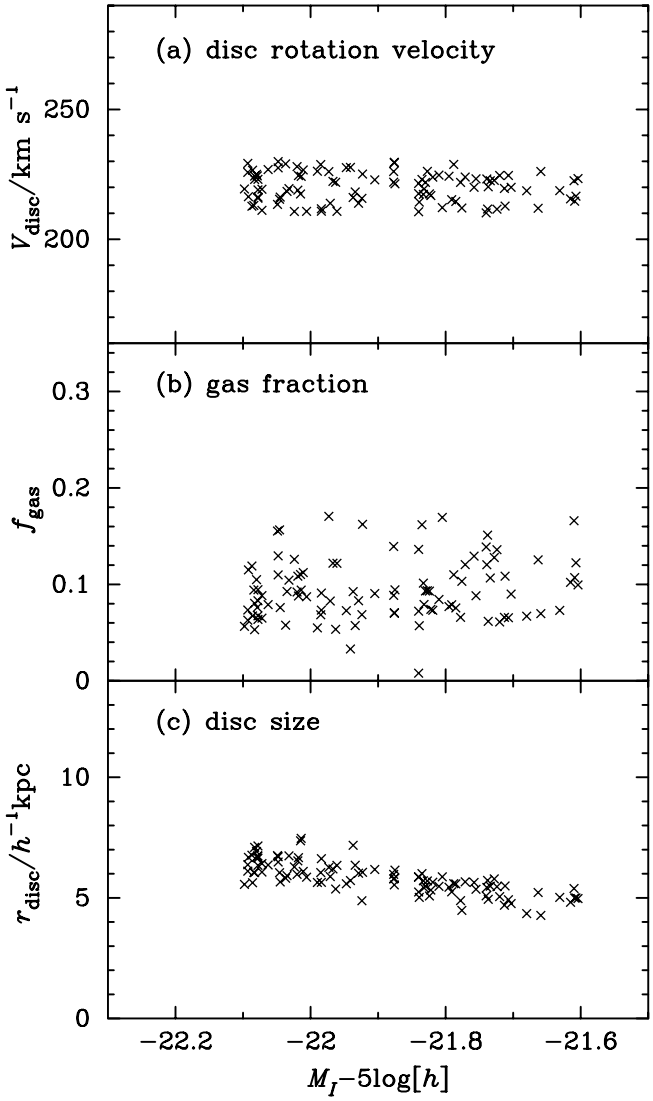

FIG. 2.—Characteristics of MW-like galaxies. The crosses indicate each MW-like galaxy. (*a*) Disk rotation velocity V_{disk}. (*b*) Cold gas fraction. (*c*) Effective radius of disks. [*See the electronic edition of the Journal for a color version of this figure*.]

surface brightness is defined as that within the effective radius. Although the lowest one is about 26 mag arcsec^{-2} (Mateo 1998), clearly observations are not a surface brightness–complete sample. As shown in Nagashima & Yoshii (2004), the lowest surface brightness of model galaxies reaches about 30 mag arcsec^{-2} in the B band at $M_B \simeq -10$. In addition, some of these low surface brightness galaxies might be disrupted by tidal interaction with other galaxies (e.g., Martin et al. 2004). These figures suggest that the so-called satellite galaxy problem might not be so serious, at least for luminous objects. Anyway, changing V_{low} and S_{th} hardly affects our results on chemical enrichment of the MW-like galaxies.

In Figure 2, we show the disk rotation velocity V_{disk}, cold gas fraction f_{gas}, and effective radius of the disk r_{disk} of the MW-like galaxies. The crosses denote individual MW-like galaxies. Since the disk rotation velocity is adjusted to be the circular velocity of the host dark halo only when the mass of the disk increases, it is not always the same as V_{circ}, which is chosen to be 220 km s^{-1} at $z = 0$. The rotation velocity obtained is distributed around the value 220 km s^{-1}, which is similar to the observed rotation velocity of the Galactic disk. The cold gas fraction is about 10%–15% in mass, and the effective radius is around 7 h^{-1} kpc. These are very similar to the observed properties of the MW. Thus, our MW-like galaxies are good enough probes to investigate the chemical enrichment in the MW.

5. COMPARISON WITH SOLAR NEIGHBORHOOD AND BULGE STARS

In this model we treat bulge and disk stars separately, so hereafter we show results for each separately, keeping in mind there are still large uncertainties in observations of bulge stars. In the following, we compare our results not only with a theoretical infall model given by Yoshii et al. (1996) but also with stars in our Galaxy. We focus on the difference between the hierarchical

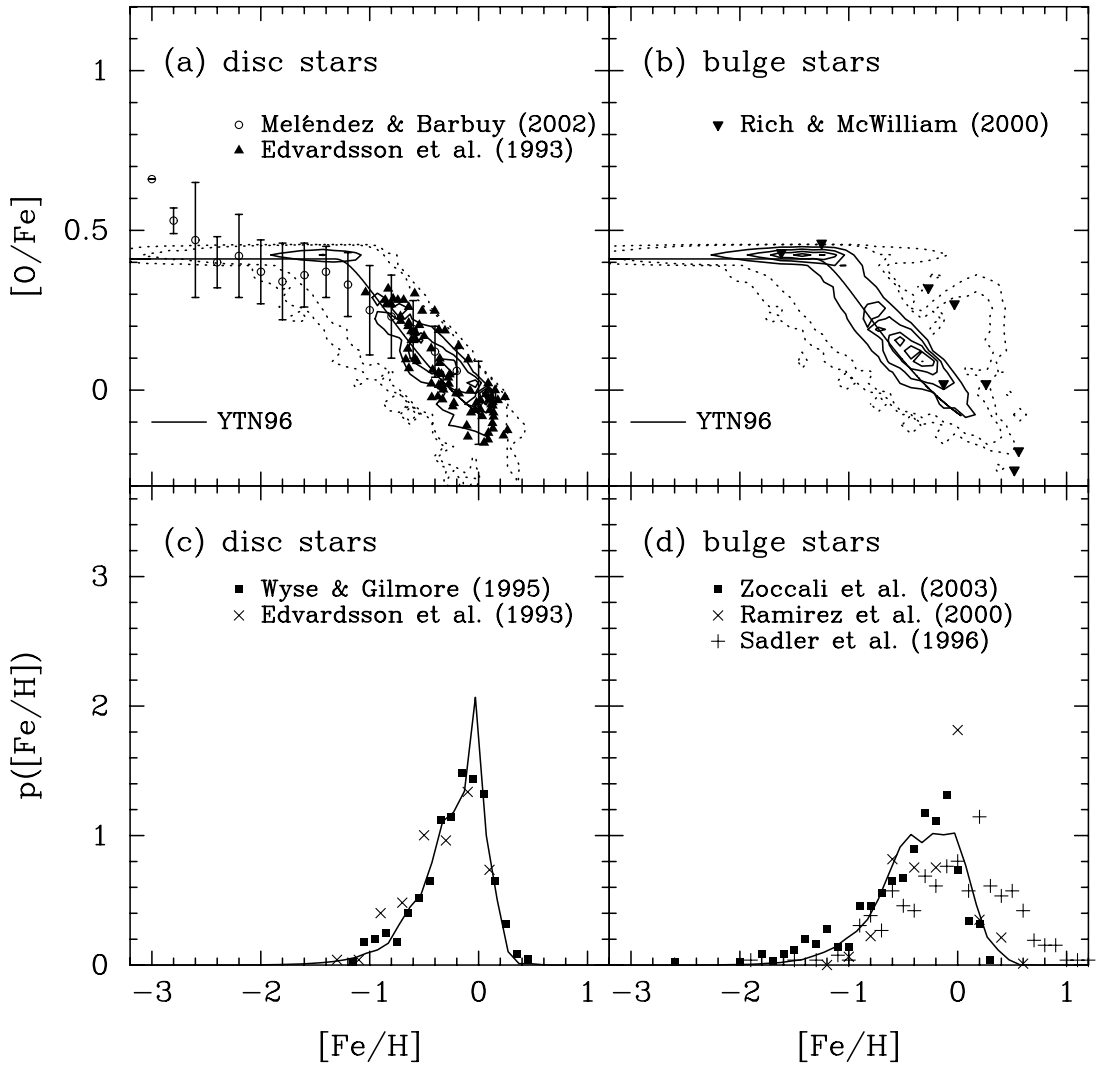

FIG. 3.—(*a*) [O/Fe] distribution against [Fe/H] for disk stars. The levels of contours drawn by the thin solid and dashed lines indicate 0.5, 0.4, 0.3, 0.2, and 0.1, and 0.02 and 0.005 times the largest number of stars in grids, respectively. The solid curve indicates a chemical enrichment model based on a monolithic cloud collapse model given by Yoshii et al. (1996). The circles with error bars and filled triangles denote observations by Meléndez & Barbuy (2002) and Edvardsson et al. (1993), respectively. (*b*) [O/Fe] distribution against [Fe/H] for bulge stars. The levels of contours and the solid curve are the same as in panel (*a*). The filled inverted triangles denote observational data by Rich & McWilliam (2000). (*c*) Iron MDF for disk stars. The solid line indicates the model prediction for disk stars. The filled squares and crosses denote observations by Wyse & Gilmore (1995) and Edvardsson et al. (1993), respectively. (*d*) Iron MDF for bulge stars. The solid line indicates the model prediction for bulge stars. The filled squares, crosses, and plus signs denote observations by Zoccali et al. (2003), Ramírez et al. (2000), and Sadler et al. (1996), respectively. [*See the electronic edition of the Journal for a color version of this figure.*]

and monolithic models, rather than comparisons with observations. We assume that our Galaxy is a representative, typical sample of MW-like galaxies under consideration. Future observations will make clear whether this assumption is valid or not.

First, in this section, we show mean properties of MW-like galaxies. Properties of individual galaxies are discussed in § 6.

In Figure 3*a* we show the distribution of disk stars in the [O/Fe]-[Fe/H] plane by contours. By tracking star formation histories and metallicity evolutions, we obtain distributions of stars in the plane for individual galaxies. The figure shows the average of 100 MW-like galaxies. The levels of contours drawn by the thin solid and dashed lines indicate 0.5, 0.4, 0.3, 0.2, and 0.1, and 0.02 and 0.005 times the largest number of stars in grids, respectively. The solid lines indicate the $k = 1$ model given by Yoshii et al. (1996; see Tables 1 and 2 in their paper for details). The crosses and filled triangles are observed data for solar neighborhood stars given by Meléndez & Barbuy (2002) and Edvardsson et al. (1993), respectively. As is clearly shown in this panel, our model reproduces well the observations of disk stars, including their dispersion. The apparent discrepancy at $[\mathrm{Fe/H}] \lesssim -2.5$ is caused by the first nucleosynthesis constraint, $y_{\mathrm{II,O}}/y_{\mathrm{II,Fe}} = \mathrm{const}$ for all SNe II (see § 3). At the break point the model prediction gives slightly higher [O/Fe] than observations. Probably if the assumption of a constant t_{Ia} were relaxed, the abundance ratio there would decrease, as suggested by Yoshii et al. (1996). The dispersion for the model comes from dispersion in a single galaxy and that for different samples. In § 6 we show the former effect by looking at some individual galaxies.

It should be noted that small radial abundance gradients of metals in the galactic disk are suggested by observations, about -0.085 dex kpc^{-1} for iron and about -0.07 dex kpc^{-1} for oxygen (Maciel 2001). This might cause a systematic difference in the metallicity distribution when averaged over the whole disk. In that case, we would need to change the values of chemical yields, which are empirically determined by Yoshii et al. (1996)

to produce an agreement with the observations for solar neighborhood stars.

Bulge stars are also distributed like disk stars in the [O/Fe]-[Fe/H] plane, but the range is slightly different, as shown in Figure 3*b*. In particular, although the fraction is low, there are many oxygen-enhanced stars at $[Fe/H] \simeq 0$. Interestingly, Rich & McWilliam (2000) found that [O/Fe] for bulge stars, shown by filled inverted triangles, has a broadly similar trend with [Fe/H] to that for disk stars, but some of them show oxygen enhancement, $[O/Fe] \simeq 0.3$ even at $[Fe/H] \simeq 0$. Recent high-resolution spectroscopic observations of bulge stars by McWilliam et al. (2003) reveal a similar trend of [Mn/Fe] to that for disk stars. While they observed fewer than 10 stars, their observations may support our model. Clearly more samples will provide important constraints on bulge formation. Using monolithic collapse models, Matteucci & Brocato (1990) predicted more oxygen-enhanced bulge stars. To obtain this, they assumed higher star formation rates and shorter infall timescales for bulge stars than those for disk stars. In our model, some bulge stars are also formed with a very short timescale, that is, in starbursts. The difference we predict between disk and bulge stars, however, is smaller, presumably because not all bulge stars are formed by starbursts and some have been formed in progenitor galaxies. Another possibility to form oxygen-enhanced stars is a variation of the IMF. Recently the IMF for starbursts was suggested to be top-heavy compared to the IMF for the disk star formation (Baugh et al. 2005; Nagashima et al. 2005a, 2005b), which means that many more SNe II must explode than expected for Salpeter-like IMFs. Because α-elements from SNe II are likely to be produced more, metal-rich bulge stars will tend to be placed at $[O/Fe] \gtrsim 0$.

In Figures 3*c* and 3*d* we show the iron MDF for disk and bulge stars, respectively. The solid lines denote the model prediction. The filled squares and crosses in Fig. 3*c* and the filled squares, crosses, and plus signs in Fig. 3*d* indicate observed [Fe/H] distributions given by Wyse & Gilmore (1995) and Edvardsson et al. (1993) for disk stars and Zoccali et al. (2003), Ramírez et al. (2000), and Sadler et al. (1996) for bulge stars, respectively. All of these distributions are normalized so that the integration over the whole range is unity. The distribution for disk stars shows an excellent agreement with the observed distributions. Agreements in abundance ratios and MDFs are quite encouraging for modeling the formation of the galactic disk in the framework of SA models. For bulge stars, there remains discrepancy among observations themselves. Our model is consistent only with the data from Zoccali et al. (2003) and Ramírez et al. (2000). The data from Sadler et al. (1996) show more metal-rich stars than the other two and our model.

While the predicted MDF for bulge stars is rather similar to that for disk stars, the width is clearly wider than that of disk stars. The observations of bulge stars show a similar tendency to that of the model, although there still seem to be uncertainties in observations outside the range $-1 \lesssim [Fe/H] \lesssim 0$. Keeping in mind differences among observational data, the model prediction for bulge stars also agrees well with the observed data. In another approach, a recent chemodynamical simulation of the galactic bulge by Nakasato & Nomoto (2003) also predicts a distribution of stars in the [O/Fe]-[Fe/H] plane and in number against [Fe/H]. In their results, there are more oxygen-enhanced stars than in the observation by Rich & McWilliam (2000) and our prediction. At the same time, their derived [Fe/H] distribution is similar to ours, although the number of high [Fe/H] stars is a little larger. Thus, although more data will be required to constrain the model of bulge formation, we can say that both our SA model and the recent numerical simulation broadly agree with the current observations.

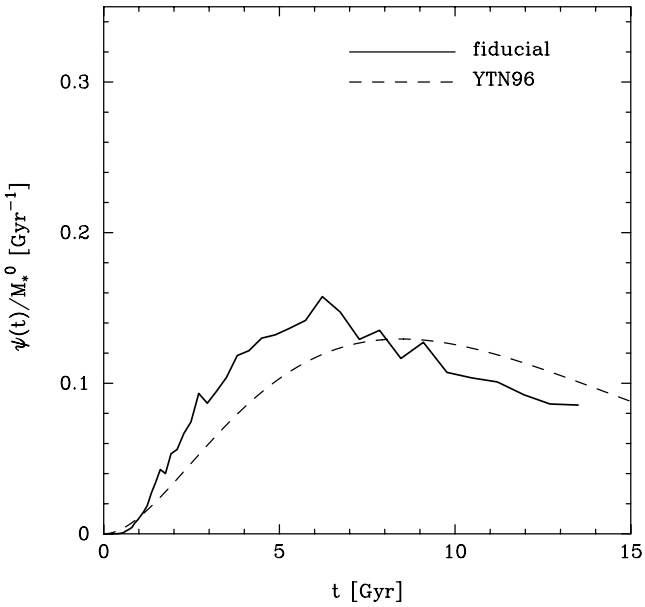

FIG. 4.—Star formation histories. The solid line indicates the averaged star formation history of MW-like galaxies. The dashed line denotes a history given by the infall model of Yoshii et al. (1996). [*See the electronic edition of the Journal for a color version of this figure*.]

Figure 4 shows averaged star formation histories of MW-like galaxies, indicated by the solid line. The infall model given by Yoshii et al. (1996) is indicated by the dashed line. Note that the star formation rate (SFR) for the infall model is plotted beyond the cosmic age given by the cosmological parameters we adopt, $\simeq$13 Gyr, because their model is normalized at 15 Gyr. The star formation rates are normalized by stellar masses at 13 Gyr. The SFRs plotted are those averaged over each time step ($\Delta M_*/\alpha\Delta t$) and over all realizations. Clearly, galaxies in our SA model have star formation histories similar to the monolithic collapse model's. Hence, the slow star formation in the infall model, which is brought about by long infall and star formation timescales chosen by obtaining an agreement with observations, is naturally explained by the mixture of physical processes including merging histories of dark halos, gas cooling, and SN feedback. While the history of each MW-like galaxy has a variety around the averaged history, as we show in § 6, we have found that predicted metallicity distributions of disk stars are quite similar to the averaged one shown in Figure 3. Since bulge components are formed by major mergers, which are rare events, it should be noted that the results on the bulge stars are just an average. Future observations of bulge stars in other galaxies will provide stronger constraints on galaxy formation models based on the CDM cosmology.

Our results suggest that the formation of spiral galaxies is well approximated by the traditional infall model, because our model provides similar results to those given by Yoshii et al. (1996). This is consistent with the result by Baugh et al. (1996), in which they traced formation histories of individual galaxies and found star formation histories of spiral galaxies similar to those of the traditional infall model (see upper panels of Fig. 3 in their paper). Note that recent infall models have become more complicated, including multiaccretion of gas, in order to reproduce observational results. Moreover, to reproduce radial gradients of metallicities, the models require SFRs dependent on the radii of disks (e.g., Chiappini et al. 1997; Fenner & Gibson

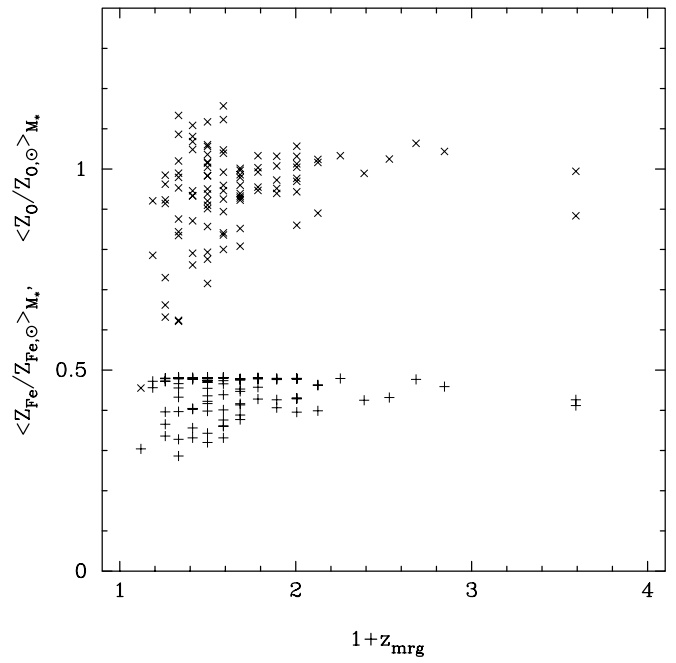

FIG. 5.—Mass-weighted metallicities of O (*crosses*) and Fe (*plus signs*) for disk stars of individual MW-like galaxies against their last major merger epochs, $z_{\rm mrg}$. [*See the electronic edition of the Journal for a color version of this figure*.]

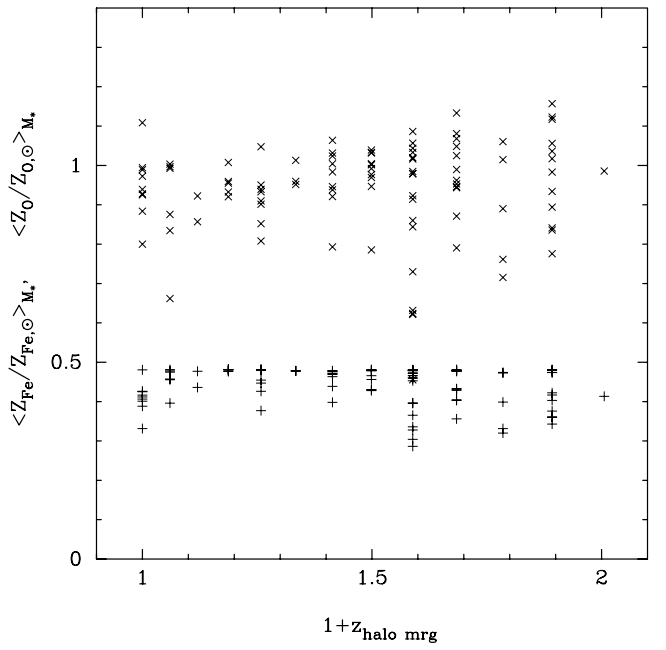

FIG. 6.—Mass-weighted metallicities of O (*crosses*) and Fe (*plus signs*) for disk stars of individual galaxies against last major merger epochs of their host halos, $z_{\rm halo\ mrg}$. [*See the electronic edition of the Journal for a color version of this figure*.]

2003). Physically, the radial gradients should be solved by computing the complex dynamics of disk formation. This requires numerical simulations of galaxy formation following the dynamical evolution including the mixing process of gas and metals.

Finally, we briefly discuss relations between averaged metallicities of individual galaxies and their merging histories. Figure 5 shows mass-weighted mean metallicities of disk stars for O (*crosses*) and Fe (*plus signs*) against their final major merger epochs, $z_{\rm mrg}$. Correlations of metallicities with $z_{\rm mrg}$ are very weak for O and negligible for Fe. In particularly, the Fe metallicity is almost independent of $z_{\rm mrg}$. The O metallicity only for galaxies that experienced a major merger very recently is slightly lower or has a larger scatter than others. To make the reason clear, however, we need more samples of high-z MW-like galaxies. The current number of high-z samples is still too few for quantitative statistical discussion. At this stage, what we can say is that there is no clear correlation between the metallicity and the final major merger epoch.

Figure 6 is the same as the previous figure, but for final major merger epochs for their host halos, $z_{\rm halo\ mrg}$. Similarly, we do not see correlations between the O metallicity and $z_{\rm halo\ mrg}$. The negligible or weaker correlation with $z_{\rm halo\ mrg}$ than with $z_{\rm mrg}$ is reasonable, because the galaxy merger does not directly reflect the halo merger and is led by other physical mechanisms, namely, dynamical friction and random collisions.

Thus, we conclude that the metallicity depends only weakly on the formation histories of galaxies and their host halos. Instead, we can see a much stronger dependence of the metallicity on parameters of, for example, SN feedback later.

6. INDIVIDUAL GALAXIES

In § 5 we showed mean properties of MW-like galaxies. Here we show results for two samples in order to see properties of individual galaxies.

Figure 7 shows luminosity functions of galaxies in two LG halos hosting MW-like galaxies as central galaxies of ID-143 with $z_{\rm mrg} = 1.13$, $z_{\rm halo\ mrg} = 0.79$, $\langle Z_{\rm O}/Z_{\rm O,\odot}\rangle = 0.89$, and $\langle Z_{\rm Fe}/Z_{\rm Fe,\odot}\rangle = 0.40$ and ID-200 with $z_{\rm mrg} = 0.59$, $z_{\rm halo\ mrg} = 0.50$, $\langle Z_{\rm O}/Z_{\rm O,\odot}\rangle = 0.99$, and $\langle Z_{\rm Fe}/Z_{\rm Fe,\odot}\rangle = 0.47$. The luminosity function in the ID-143 halo agrees well with the observed one at $M_V \lesssim -15$, and that in the ID-200 halo broadly agrees but slightly overproduces galaxies at $M_V \sim -17$. This slight discrepancy between the models and the observations should substantially

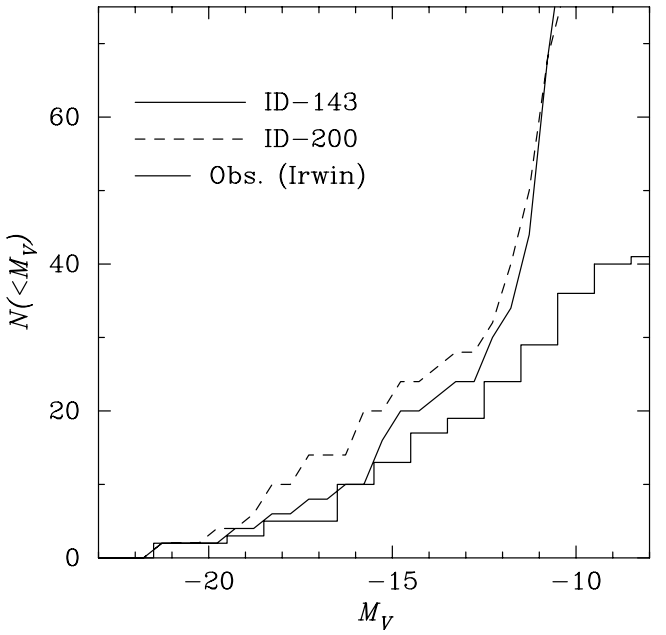

FIG. 7.—Cumulative luminosity functions in LG halos of ID-143 (*solid line*) and ID-200 (*dashed line*). No selection effect is taken into account. The histogram denotes the same observed luminosity function shown in Fig. 1. [*See the electronic edition of the Journal for a color version of this figure*.]

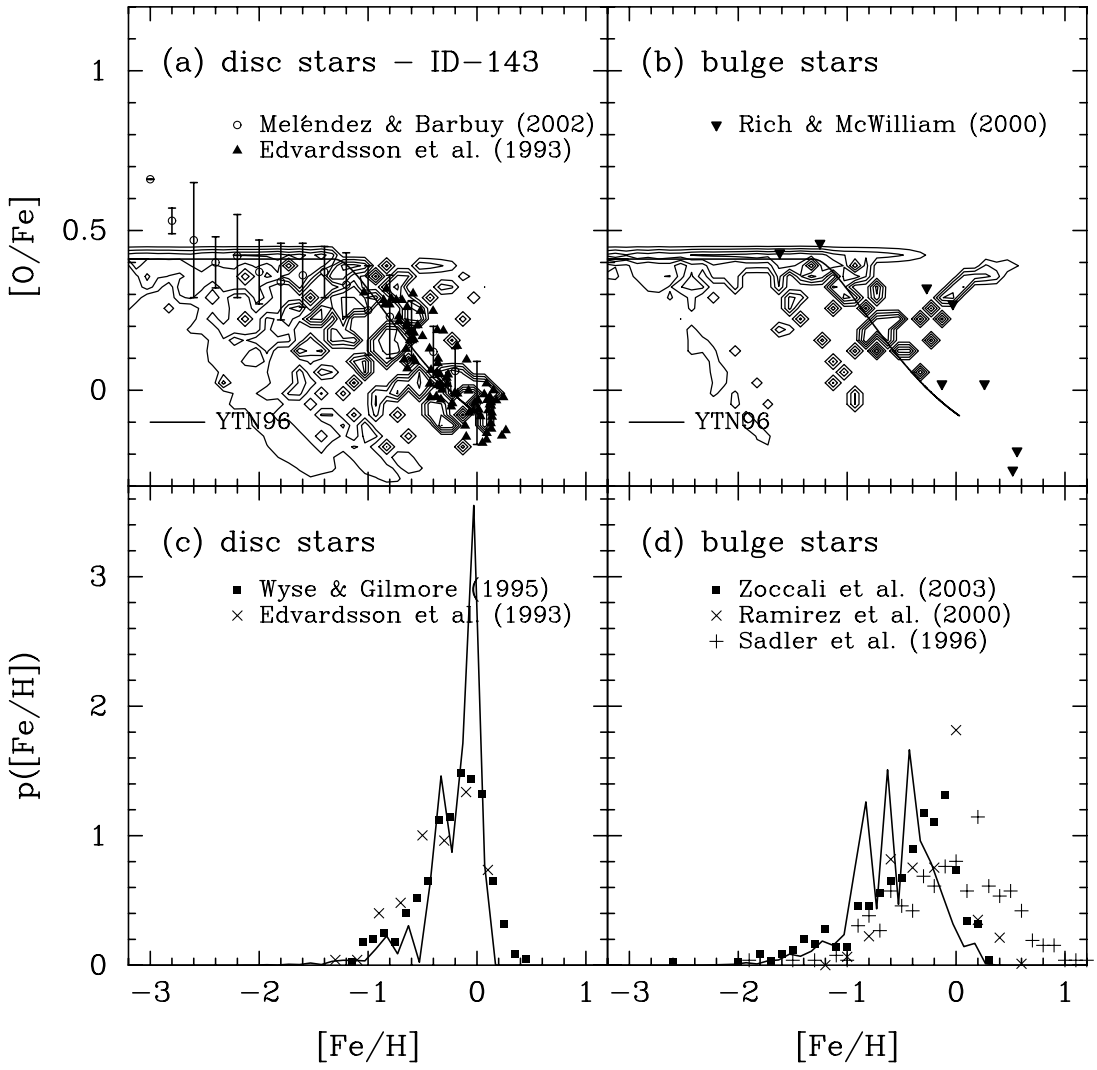

FIG. 8.—Same as Fig. 3, but for a MW-like galaxy of ID-143. Note that in order to enhance contribution of stars with small fractions, the contour levels are equally divided logarithmically. [*See the electronic edition of the Journal for a color version of this figure*.]

decrease when taking into account effects such as the selection effects shown in § 4. We also find that difference between samples is not significant.

Figures 8 and 9 show the same figures as Figure 3, that is, the distribution of disk and bulge stars in the [O/Fe]-[Fe/H] plane and MDFs for [Fe/H], but for individual galaxies of ID-143 and ID-200, respectively. In order to enhance the contribution of stars with small fractions, the contour levels are not linear but logarithmic. As can easily be seen, some stars are located in a low-[O/Fe] region at low [Fe/H], particularly for ID-143. Such stars can be brought by smaller subclumps via minor mergers. Because low-mass galaxies with shallow gravitational potential wells suffer strong SN feedback, the metal enrichment does not proceed significantly. Therefore, SNe Ia start to explode and lower [O/Fe] when [Fe/H] is still low. This effect is shown in Figure 16 for a stronger SN feedback case. Although the number of such stars is small, they might be discovered as relics of past minor merger histories. Note that, of course, this depends on the details of the process of minor mergers.

In contrast to ID-143, the galaxy ID-200 does not have such low-[O/Fe], low-[Fe/H] disk stars. This is because minor mergers did not happen after the last major merger, and the disk grew in a similar way to the infall model of monolithic collapse. Merging histories of these galaxies should provide insights for understanding the difference in the stellar distribution in the [O/Fe]-[Fe/H] plane. For example, the last merger epoch for this galaxy is $z_{\rm mrg} = 0.59$, and for the ID-143 galaxy with many minor mergers $z_{\rm mrg} = 1.13$, which is earlier than that of ID-200. Thus, it should have been hard for the ID-200 galaxy to accrete small subclumps as minor mergers until the present.

Similar trails can be seen for bulge stars of both the ID-143 and ID-200 galaxies, in contrast to disk stars. Because many stars in bulges formed in disks first and then were transferred to bulges by major mergers, the trails in bulges should reflect minor-merger histories onto disks before the formation of bulges, or, the last major mergers. Therefore, these galaxies could have enough time to accrete subclumps until the last major mergers.

The widths of MDFs for both MW-like galaxies are slightly narrower than the averaged one shown in Figure 3. In our model we assume that metals are well mixed in a galaxy. In reality, however, the mixing of metals in a galaxy would not be completed, and therefore the MDF would be broadened, as observed. If we take this effect of inhomogeneous metal enrichment into account, the MDF will become wider. Note that recent observations of more than 10,000 solar neighborhood stars by Nordström et al. (2004) have suggested a narrower MDF than past observations.

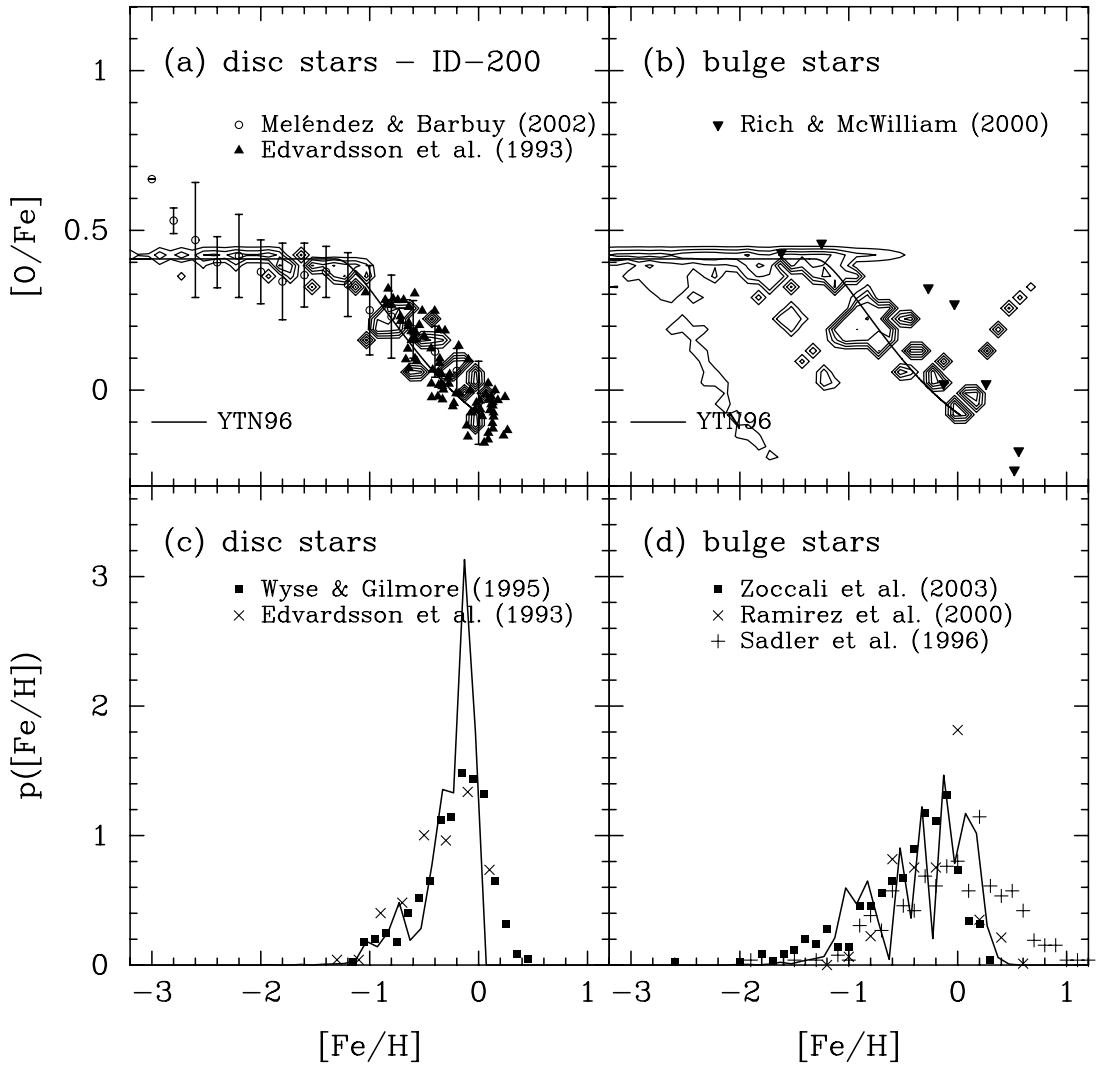

FIG. 9.—Same as Fig. 8, but for a MW-like galaxy of ID-200. [*See the electronic edition of the Journal for a color version of this figure.*]

Although we should be careful in sample selection, this may suggest that the metal mixing is efficient for disk stars. This should be addressed in the future.

7. PARAMETER DEPENDENCE

Here we investigate how the stellar metallicity depends on the fundamental model parameters, such as the SN feedback and star formation timescale, as well as the lifetime of SNe Ia, in order to clarify how physical processes such as star formation affect chemical enrichment in galaxies. Note that the parameters adopted below break the agreement with observations. We vary the values of the parameters just to see how each physical process affects metal enrichment.

7.1. *Lifetime of SNe Ia*

First, we vary the lifetime of SNe Ia, $t_{\rm Ia}$. In Figures 10 and 11 we show the same model as in Figure 3, but for $t_{\rm Ia} = 0.5$ and 3 Gyr, respectively. In the case of the shorter $t_{\rm Ia}$, because enrichment due to SNe Ia begins earlier, the break point in the [O/Fe]-[Fe/H] plane moves toward lower [Fe/H]. On the other hand, in the longer $t_{\rm Ia}$ case, the iron abundance initially increases only due to SNe II, so the break point moves toward higher [Fe/H]. This dependence is basically the same as that shown in analyses using the traditional model. This also suggests the similarity of formation of spiral galaxies between the hierarchical and traditional models.

In the shorter $t_{\rm Ia}$ case, an interesting feature in abundance ratio emerges. Bulge stars have a kind of U-shaped distribution with a minimum at [Fe/H] ~ -0.5 in the [O/Fe]-[Fe/H] plane. In this case, iron enrichment due to SNe Ia is almost completed at very high redshift, at which time a large amount of cold gas remains in galaxies. Hence, most of the stars existing at present form in subsequent starbursts due to major mergers between such gas-rich systems. Because a starburst tends to make stars in its late phase with the abundance pattern of SNe II, if the system is gas-rich, many oxygen-enhanced iron-rich stars form during the starburst. Thus, this provides a constraint on the lifetime of SNe Ia, that is, $t_{\rm Ia}$ should be rather long, $\gtrsim$1 Gyr.

The dependence of the [Fe/H] distribution on $t_{\rm Ia}$ is not as simple as that of the abundance ratio. These figures show that the lifetime $t_{\rm Ia}$ seems to determine the width of the [Fe/H] distribution, that is, a shorter $t_{\rm Ia}$ makes the [Fe/H] distribution narrower. This could be related to the epoch of star formation. In the shorter $t_{\rm Ia}$ case, many intermediate stars explode as SNe Ia and begin to release metals into the interstellar medium before the major epoch of star formation, compared with the reference model; therefore, most of the stars have similar iron abundances, which

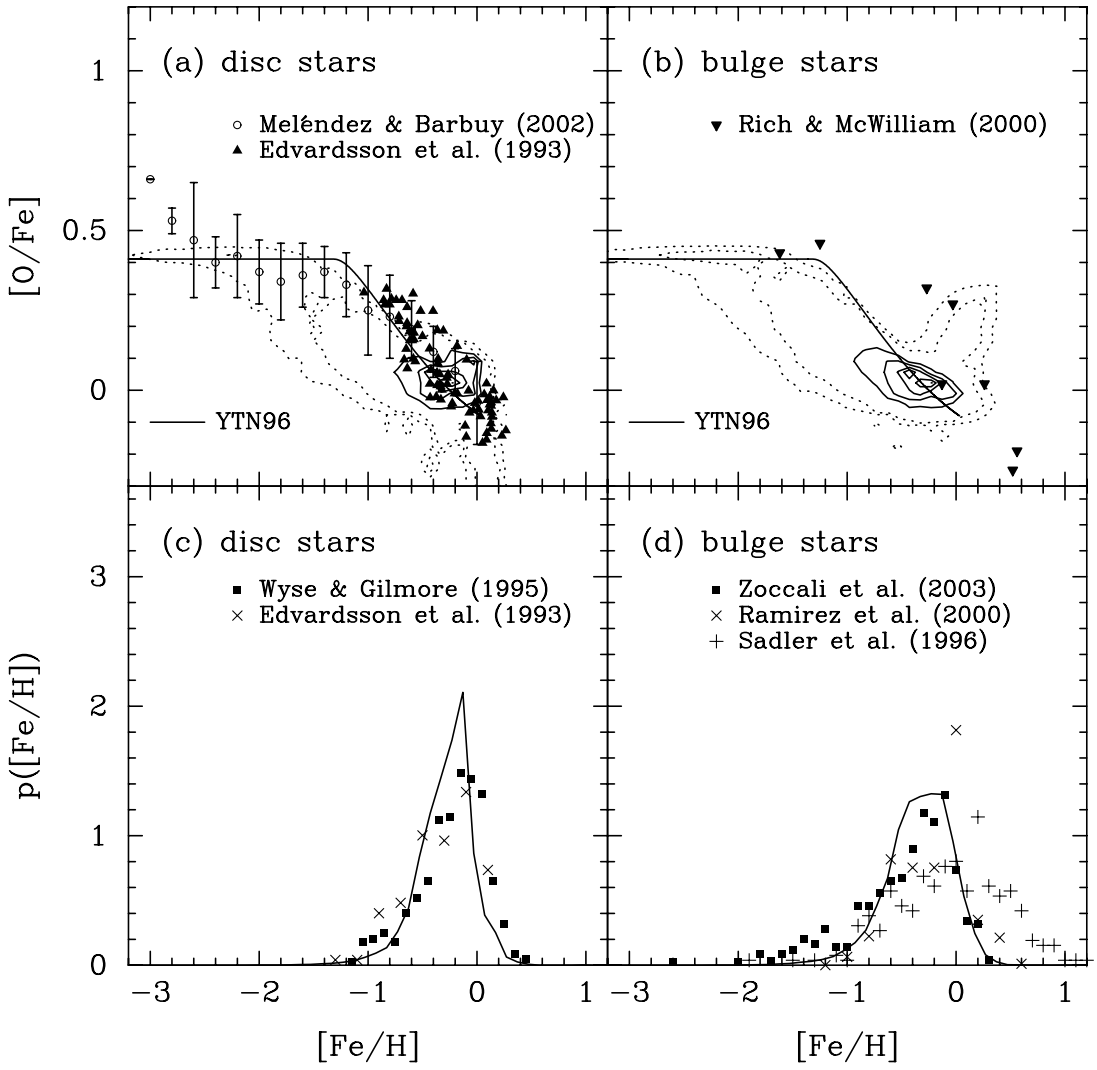

FIG. 10.—Same as Fig. 3, but for $t_{\rm Ia} = 0.5$ Gyr. [*See the electronic edition of the Journal for a color version of this figure.*]

makes the [Fe/H] distribution narrow. In contrast, in the longer $t_{\rm Ia}$ case some of the stars form in iron-poor environments before most of the iron is released, and some of the stars form in iron-rich environments because at late epochs the gas fraction is low and iron is released into gas-poor systems. Thus, the [Fe/H] distribution has a wider width.

7.2. *Star Formation Timescale*

Next, we investigate the dependence on the star formation timescale. In Figures 12 and 13 we show models that are the same as the reference model, except for having twice and half the star formation timescale of the reference model, $\tau_*^0 = 2.6$ and 0.65 Gyr, respectively.

As seen in Figure 12*b*, in the longer star formation timescale case the break point in the [O/Fe]-[Fe/H] plane for bulge stars moves toward lower [Fe/H], because the star formation epoch shifts to lower redshift and then the enrichment due to SNe Ia effectively begins earlier. In the case of a shorter star formation timescale, by contrast, the break point moves toward higher [Fe/H]. Thus, we can say that the position of the break point is generally determined by a combination of the lifetime of SNe Ia and the star formation timescale, such as $t_{\rm Ia}/\tau_*^0$. In the longer τ_*^0 case, there is a broader tail showing oxygen enhancement at [Fe/H] ~ 0 than in the reference model. This is for the same reason as in the case of shorter $t_{\rm Ia}$. The difference from the case with shorter $t_{\rm Ia}$ is that the distribution is not U-shaped but an inverted triangle, because the SNe Ia continue enrichment at lower redshifts. Disk stars also have the same dependence on the star formation timescale, but we can clearly see those tendencies for bulge stars.

The [Fe/H] distribution shows a different tendency from the dependence on $t_{\rm Ia}$. In the case of longer and shorter τ_*^0, the distributions typically, but slightly, have lower and higher [Fe/H], respectively, at least for bulge stars. Generally, a longer star formation timescale results in a larger cold gas fraction. Then, with the longer star formation timescale, the metallicity becomes lower than in a model with a shorter star formation timescale. In addition, such a longer star formation timescale decreases the amount of stars, which means that fewer metals are released from SNe Ia. Thus, the star formation timescale has a different effect from the lifetime of SNe Ia.

In the reference model, the star formation timescale is assumed to be constant with redshift. It is interesting to see how the redshift dependence affects the chemical enrichment. In Nagashima & Yoshii (2004), another formulation for the star formation timescale is considered; it is proportional to the dynamical

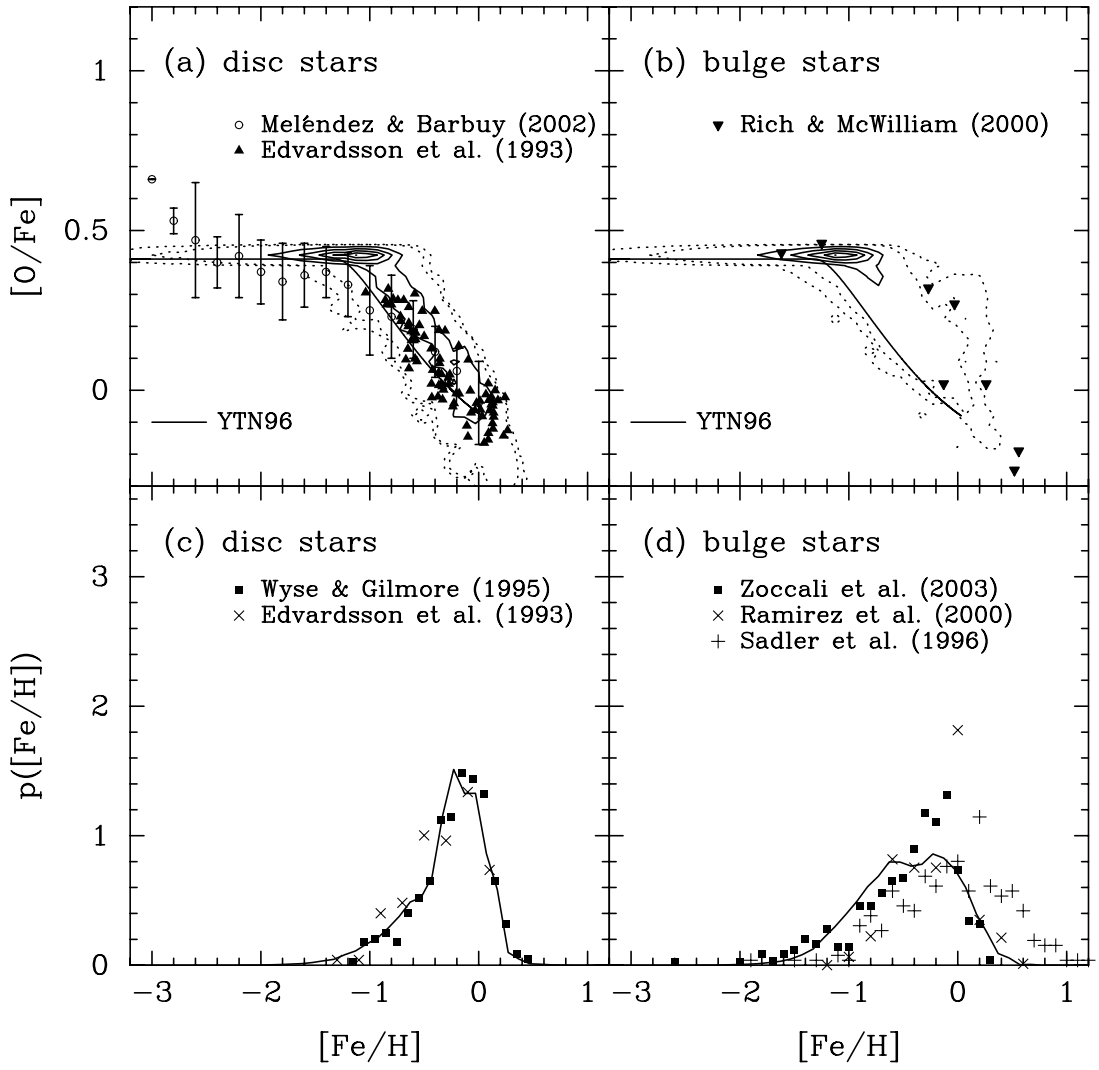

FIG. 11.—Same as Fig. 3, but for $t_{\rm Ia} = 3$ Gyr. [*See the electronic edition of the Journal for a color version of this figure.*]

timescale of the galactic disk, which is called the dynamical star formation (DSF) timescale model in that paper. Because we assume the disk rotation velocity to be almost the same as the circular velocity of dark halos, which becomes larger toward higher redshift, the dynamical timescale becomes shorter toward higher redshift. Figure 14 shows the results of adopting the DSF model, in which the star formation timescale at present is $\tau_*^0 =$ 1.7 Gyr, so as to produce an agreement of the cold gas fraction in spiral galaxies with observations. We find that the position of the break point in the [O/Fe]-[Fe/H] plane moves slightly toward higher [Fe/H], and the slope of [O/Fe] against [Fe/H] seems to be slightly steeper. In the DSF model, since most stars form at higher redshift than in the reference model due to the shorter star formation timescale at high redshift, enrichment of iron happens quickly. Thus, the slope is steeper, and the typical [Fe/H] is larger than in the reference model, but this effect is very small.

In Figure 15 we show star formation histories of those three models. The solid, dot-dashed, and dotted lines indicate models with $\tau_*^0 = 2.6$ and 0.65 Gyr and the DSF model, respectively. The dashed line denotes the infall model given by Yoshii et al. (1996). The major star formation epochs of the models of $\tau_*^0 = 2.6$ and 0.65 Gyr are later and earlier than the reference model shown in Figure 4. Because a star formation timescale at high redshift in the DSF model is much shorter than that in the reference model, the major star formation epoch moves toward an even earlier epoch than the model of $\tau_*^0 = 0.65$ Gyr. From this figure, we can thus reach the same conclusion as analyses by the infall model, that is, when major star formation finishes before iron enrichment due to SNe Ia becomes efficient, the break point in [O/Fe]-[Fe/H] moves toward higher [Fe/H], because even SNe II alone sufficiently enrich stars.

As long as we vary only the lifetime of SNe Ia, $t_{\rm Ia}$, and the star formation timescale, τ_*, our SA model seems to provide quite similar conclusions to the classical infall model. This apparent coincidence, however, breaks when the SN feedback is considered, as shown in § 7.3.

7.3. *Supernova Feedback*

It has been widely realized that SN feedback significantly affects galaxy properties. Strong energy feedback suppresses chemical enrichment due to SNe II, because star formation is suppressed by expelling cold gas, and also most of the metals are expelled into the hot gas (Kauffmann & Charlot 1998; Nagashima & Gouda 2001). Thus, it is worthwhile to investigate how SN feedback affects the enrichment due to both SNe II and SNe Ia.

In Figures 16 and 17 we show the same figures as Figure 3, but for $V_{\rm hot} = 280$ (strong feedback) and 70 (weak feedback) km s^{-1},

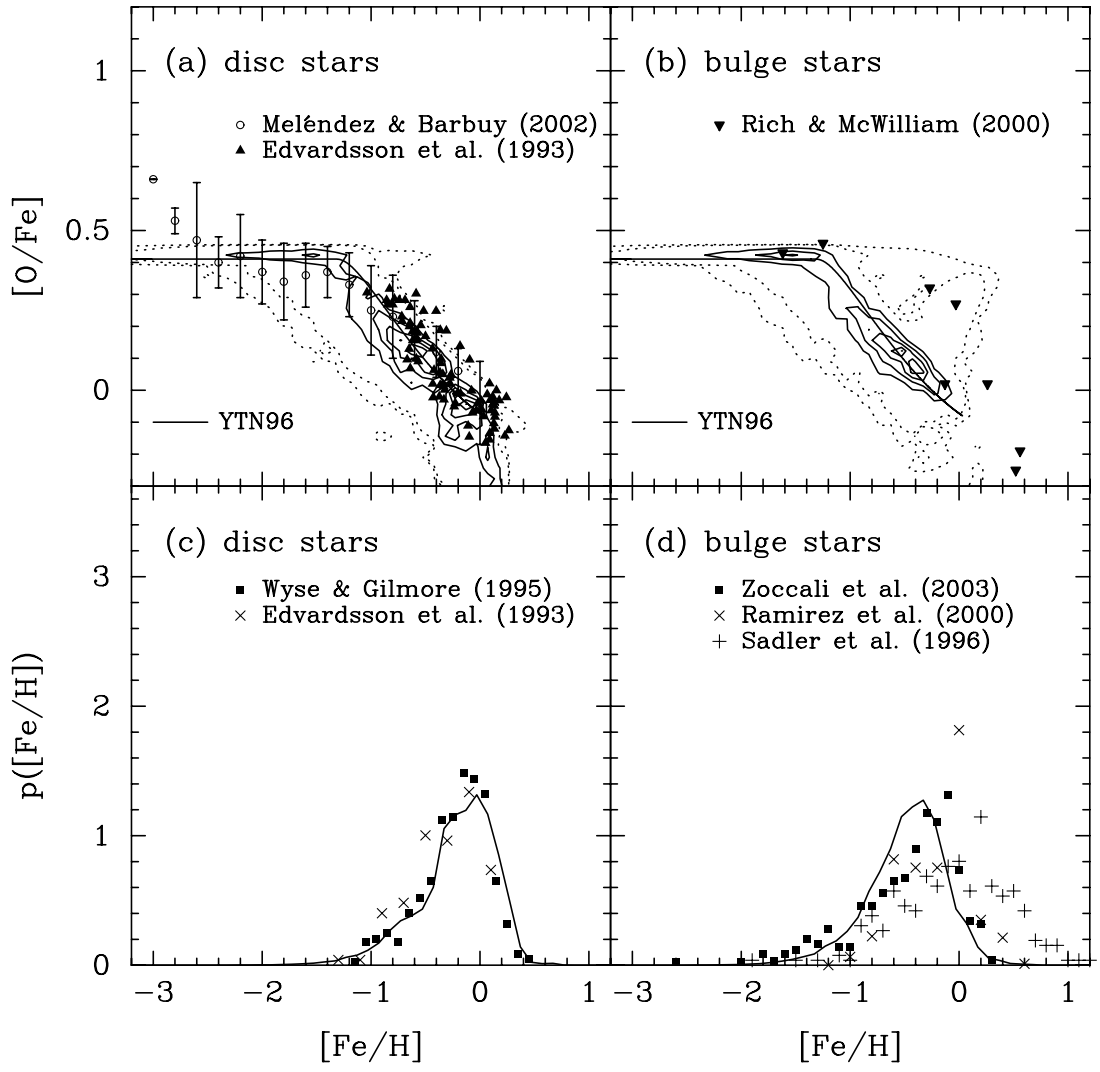

FIG. 12.—Same as Fig. 3, but for $\tau_*^0 = 2.6$ Gyr. [*See the electronic edition of the Journal for a color version of this figure.*]

respectively, where $V_{\rm hot}$ determines the typical scale at which SN feedback becomes effective, that is, SN feedback strongly affects galaxies with $V_{\rm disk} < V_{\rm hot}$. As clearly shown in the bottom panels, the [Fe/H] distributions for both disk and bulge stars are strongly affected by SN feedback. Strong feedback greatly suppresses formation of metal-rich stars and thus the chemical enrichment. In contrast, there are too few metal-poor stars in the case of weak SN feedback compared with the observed distributions, while the difference from the reference model is smaller than that of the strong SN feedback case. It should be noted that our MW-like galaxies have $V_{\rm disk} \simeq 220$ km s^{-1} at low redshift. The values of $V_{\rm hot}$ for both the reference model and the weak SN feedback case are less than the rotation velocity, while in the strong SN feedback case $V_{\rm hot}$ is larger than the rotation velocity. That means that SN feedback is very efficient even at low redshift in the strong feedback case. Therefore, the difference of the strong SN feedback case from the reference model is larger.

The stronger the SN feedback is, the lower the [Fe/H] at the break point is. Consequently, strong and weak SN feedback seem to have similar effects in the [O/Fe]-[Fe/H] plane to those of short and long $t_{\rm Ia}$ and long and short τ_*^0. Since strong SN feedback suppresses the chemical enrichment due to SNe II, the enrichment due to SNe Ia begins at a lower [Fe/H]. These apparently correspond to longer and shorter star formation timescales, respectively.

Figure 18 shows star formation histories of the strong ($V_{\rm hot} = 280$ km s^{-1}) and weak ($V_{\rm hot} = 70$ km s^{-1}) feedback models indicated by the solid and dot-dashed lines, respectively. The dashed line denotes the infall model. The strong feedback model shows a similar star formation history to that of the long star formation timescale model (the solid line in Fig. 15). Both models have break points in the [O/Fe]-[Fe/H] plane at slightly lower [Fe/H] than that in the reference model. The peak of the [Fe/H] distribution of the strong feedback model, however, moves toward lower [Fe/H] compared with the long star formation timescale model.

The weak feedback model shows a similar star formation history to that of the DSF model (the dotted line in Fig. 15). The break points of both models move toward high [Fe/H] compared with the reference model. Again, the shift to higher [Fe/H] in the [Fe/H] distribution of the weak feedback model is slightly enhanced compared with the DSF model.

This is because SN feedback strongly affects chemical enrichment. From equations (5)–(8), we obtain a mass-weighted mean stellar metallicity,

$$\langle Z_*(t)\rangle = Z_c^0 + \frac{\alpha y}{\alpha+\beta}\frac{1-e^{-x}-xe^{-x}}{1-e^{-x}}, \qquad (10)$$

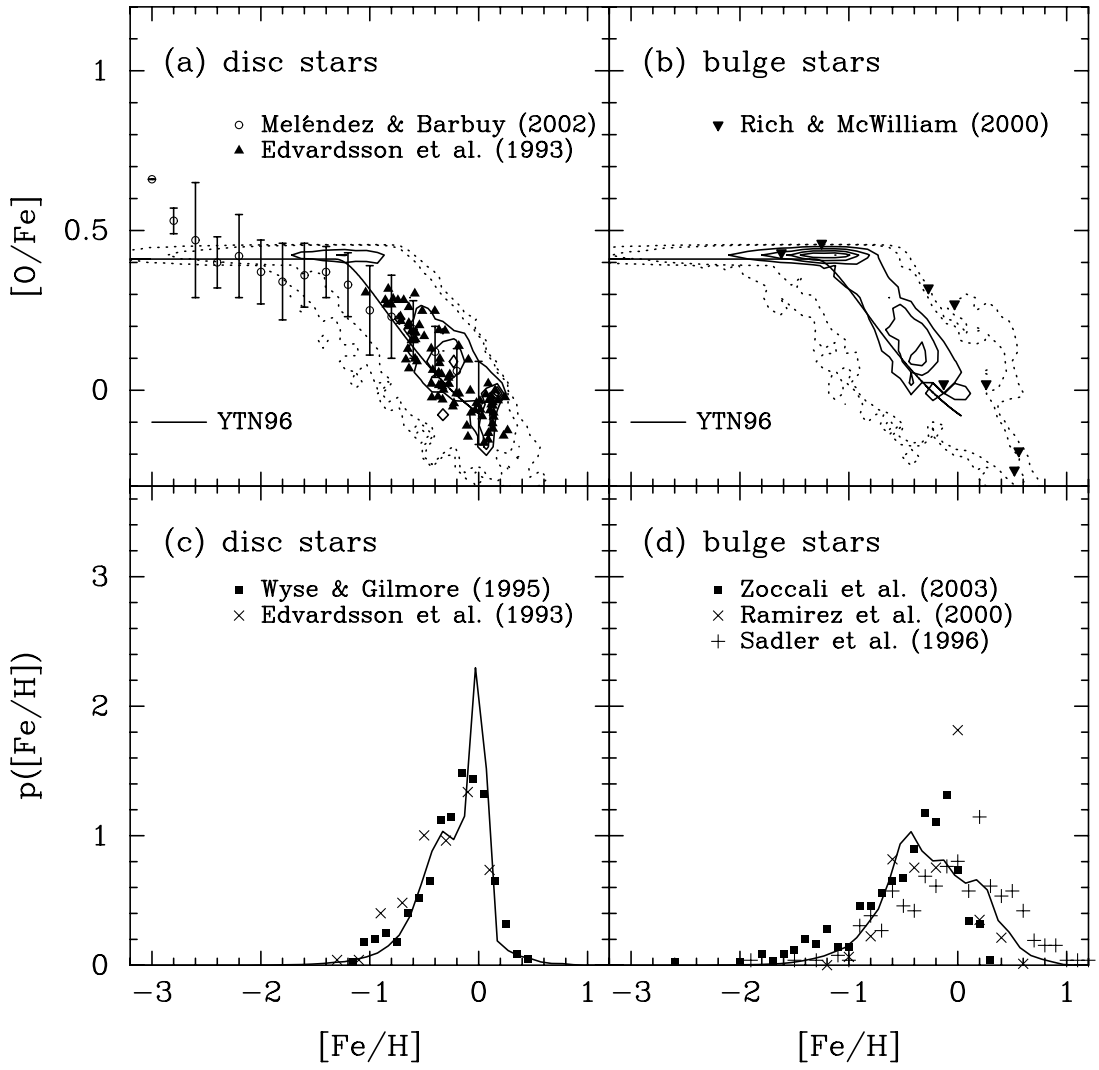

FIG. 13.—Same as Fig. 3, but for $\tau_*^0 = 0.65$ Gyr. [*See the electronic edition of the Journal for a color version of this figure.*]

where $x = (\alpha + \beta)t/\tau_*$ and Z_c^0 is an initial metallicity of gas. At the limit $t/\tau_* \rightarrow \infty$, the mean metallicity becomes

$$\langle Z_*(\infty)\rangle \rightarrow Z_c^0 + \frac{\alpha y}{\alpha + \beta}. \tag{11}$$

This shows that a strong SN feedback ($\beta \gg 1$) suppresses chemical enrichment due to SNe II. The effective chemical yield taking into account SN feedback can be written as $y_{\rm eff} = y/(1 + \beta/\alpha)$. The effect of SN feedback on chemical enrichment is the reason why, for example, the strong feedback model and the long star formation timescale model predict different [Fe/H] distributions in spite of their similar star formation histories. Therefore, similar star formation histories do not always provide similar chemical enrichment histories. Gas outflow induced by SNe II plays a critical role in galaxy evolution.

8. SUMMARY

We have explored chemical enrichment due to both SNe II and SNe Ia in Milky Way–like galaxies in the semianalytic galaxy formation model. Our treatment of SNe Ia is fully consistent with the galaxy formation model, that is, we solve for the recycling of each element among stars, cold gas, and hot gas based on a ΛCDM model. It is important to follow the chemical enrichment in the framework of the hierarchical galaxy formation, because there are many nontrivial effects on the chemical enrichment caused not only by mergers of galaxies but by varying efficiencies of the SN feedback dependent on the depth of gravitational potential wells of subgalactic clumps. As a first attempt at constructing such a consistent model, we have assumed that all SNe Ia have the same lifetime, $t_{\rm Ia}$, that abundance patterns of metals from SNe Ia and SNe II are always the same, and that massive stars instantaneously explode as SNe II and release metals. This is a natural extension of the work by Yoshii et al. (1996), in which they self-consistently modeled the chemical enrichment due to SNe Ia and SNe II.

We have picked out galaxies in dark halos with $V_{\rm circ} = 220$ km s^{-1} and having a similar luminosity to the MW. We have found that when we impose $t_{\rm Ia} = 1.5$ Gyr, the predictions of our model for such MW-like galaxies agree well with observations of the chemical composition of solar neighborhood stars both in the stellar distribution in the [O/Fe]-[Fe/H] plane and in the iron MDF. We would like to stress that the other model parameters such as the star formation timescale and SN feedback are the same as in the fiducial model of Nagashima & Yoshii (2004), in which they found that the model reproduced well many aspects of observed galaxies, such as luminosity functions, cold

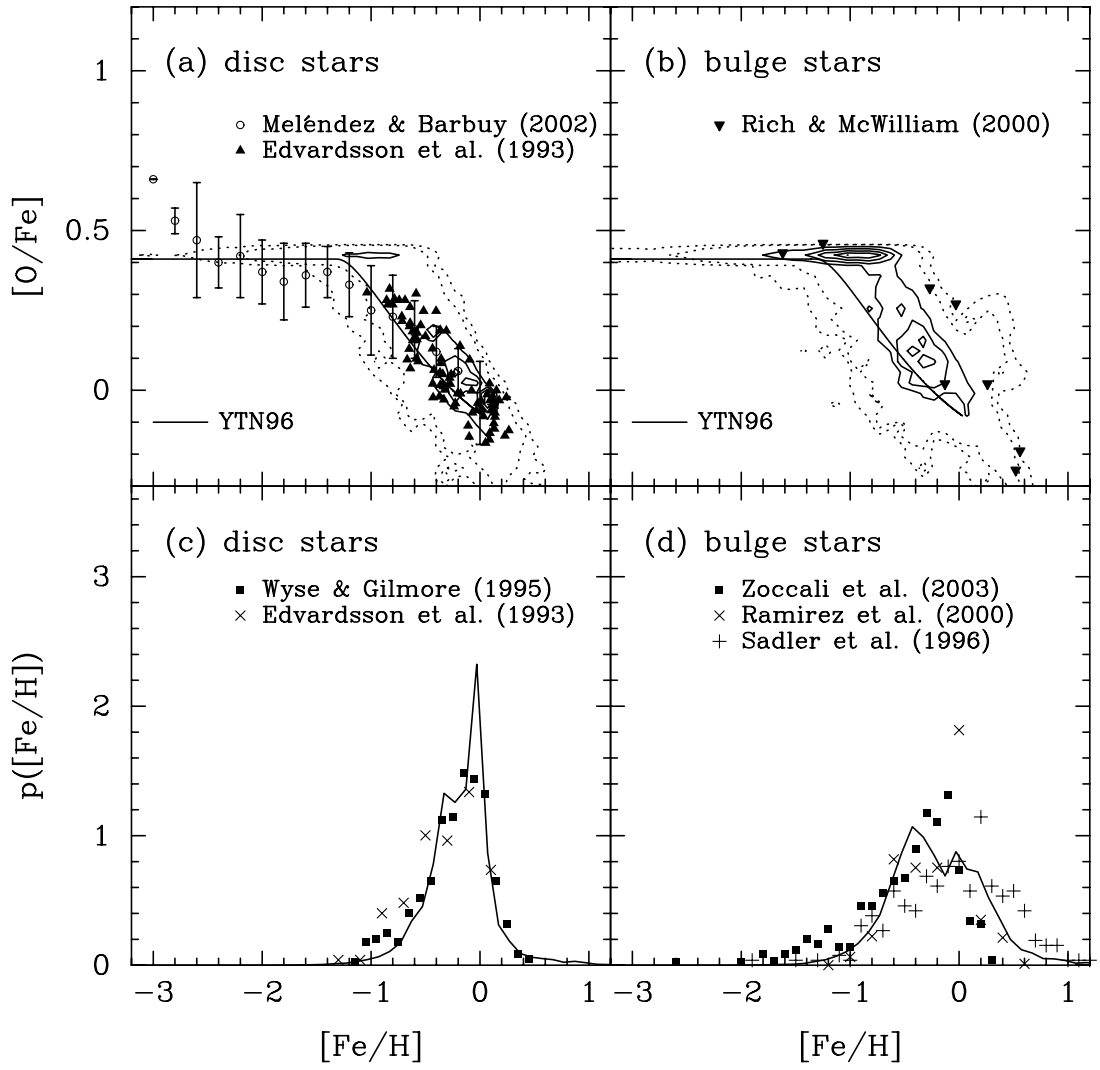

FIG. 14.—Same as Fig. 3, but for the DSF model. [*See the electronic edition of the Journal for a color version of this figure.*]

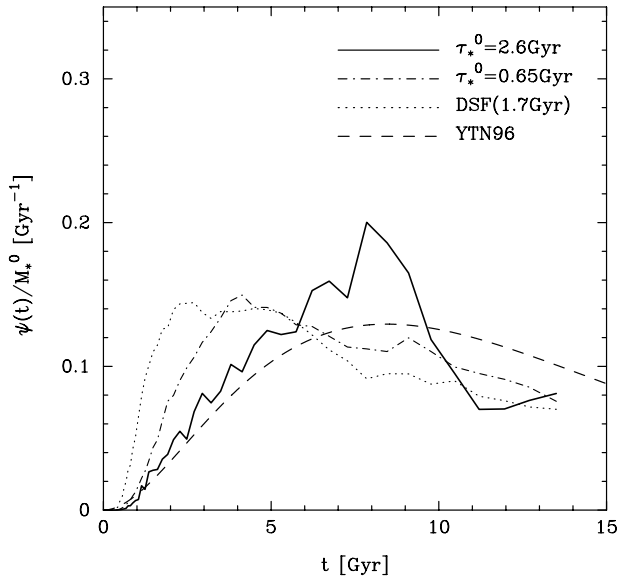

FIG. 15.—Star formation histories. The solid, dot-dashed, and dotted lines indicate models with $\tau_*^0 = 2.6$ and 0.65 Gyr and a model with DSF, respectively, corresponding to Figs. 12, 13, and 14. The dashed line denotes the infall model. [*See the electronic edition of the Journal for a color version of this figure.*]

gas fractions, and sizes of galaxies for local galaxies and the surface brightnesses, velocity dispersions, mass-to-light ratios, and metallicities of local dwarf spheroidals. This work also shows that the classical G dwarf problem (van den Bergh 1962; Schmidt 1963; Pagel & Patchett 1975) is fully resolved in the framework of hierarchical formation of galaxies, in which the infall term introduced in the infall models to avoid the G dwarf problem is naturally explained by the mixture of such physical processes as clustering of dark halos, gas cooling, and SN feedback. Our model passes the new tests, that is, the iron MDF and the abundance pattern of metals, taking into account chemical enrichment due to SNe Ia. As shown in § 7, the abundance pattern provides an independent constraint on galaxy formation. Therefore, our results would support the scenario of hierarchical formation of galaxies. While observational data used in this work have been limited to solar neighborhood and bulge stars in the Milky Way, future observations of stars in other galaxies will provide statistically better constraints on galaxy formation.

In our model, disk and bulge stars are treated separately. While the observations of bulge stars still have uncertainties, our model also reproduces well both the distribution of stars in the [O/Fe]-[Fe/H] plane and the [Fe/H] distribution. In particular, although there are only a few bulge stars whose oxygen abundance is observed, our model predicts oxygen-enhanced stars at [Fe/H] ~ 0,

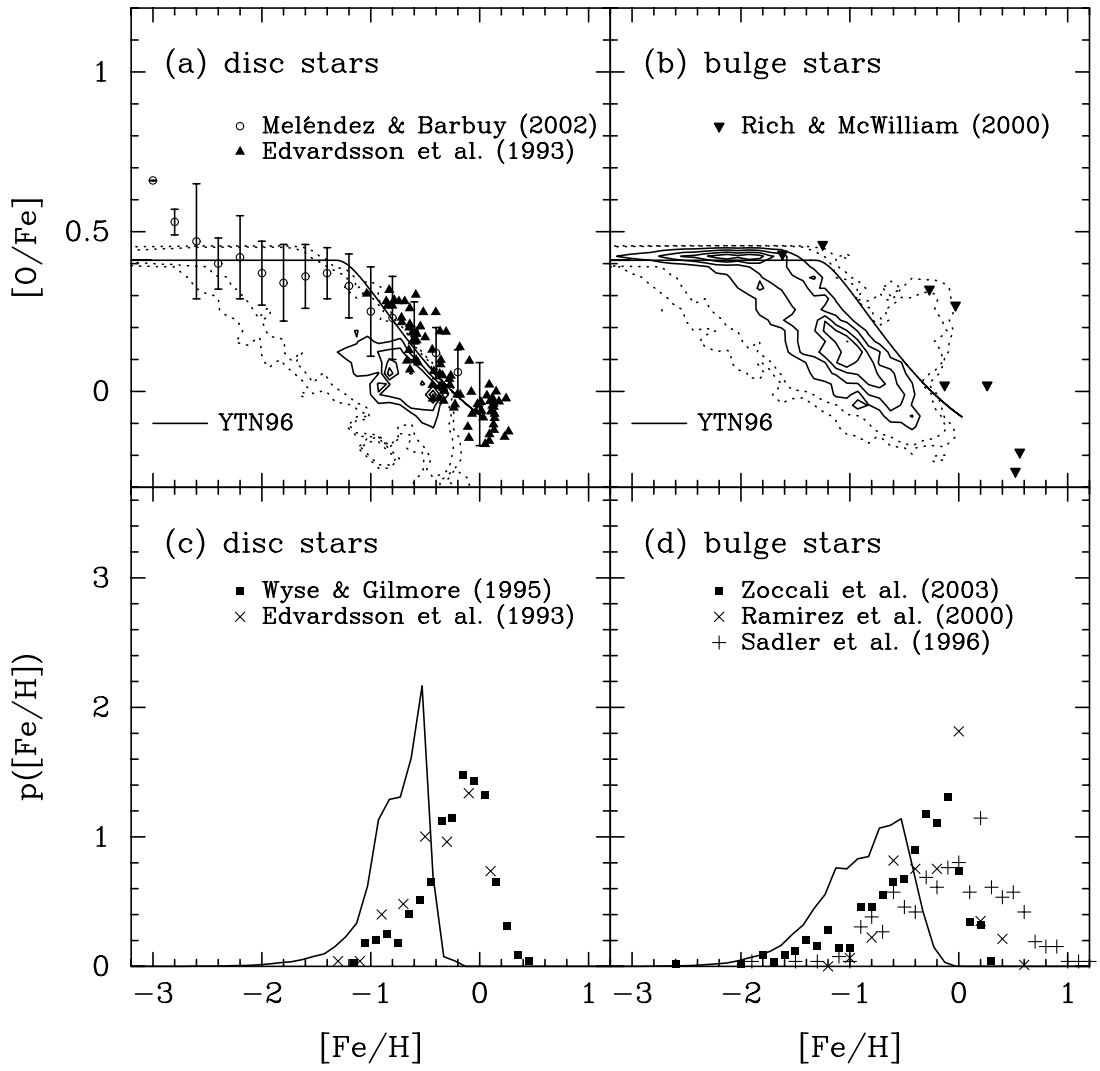

FIG. 16.—Same as Fig. 3, but for $V_{\rm hot} = 280$ km s^{-1}. [*See the electronic edition of the Journal for a color version of this figure.*]

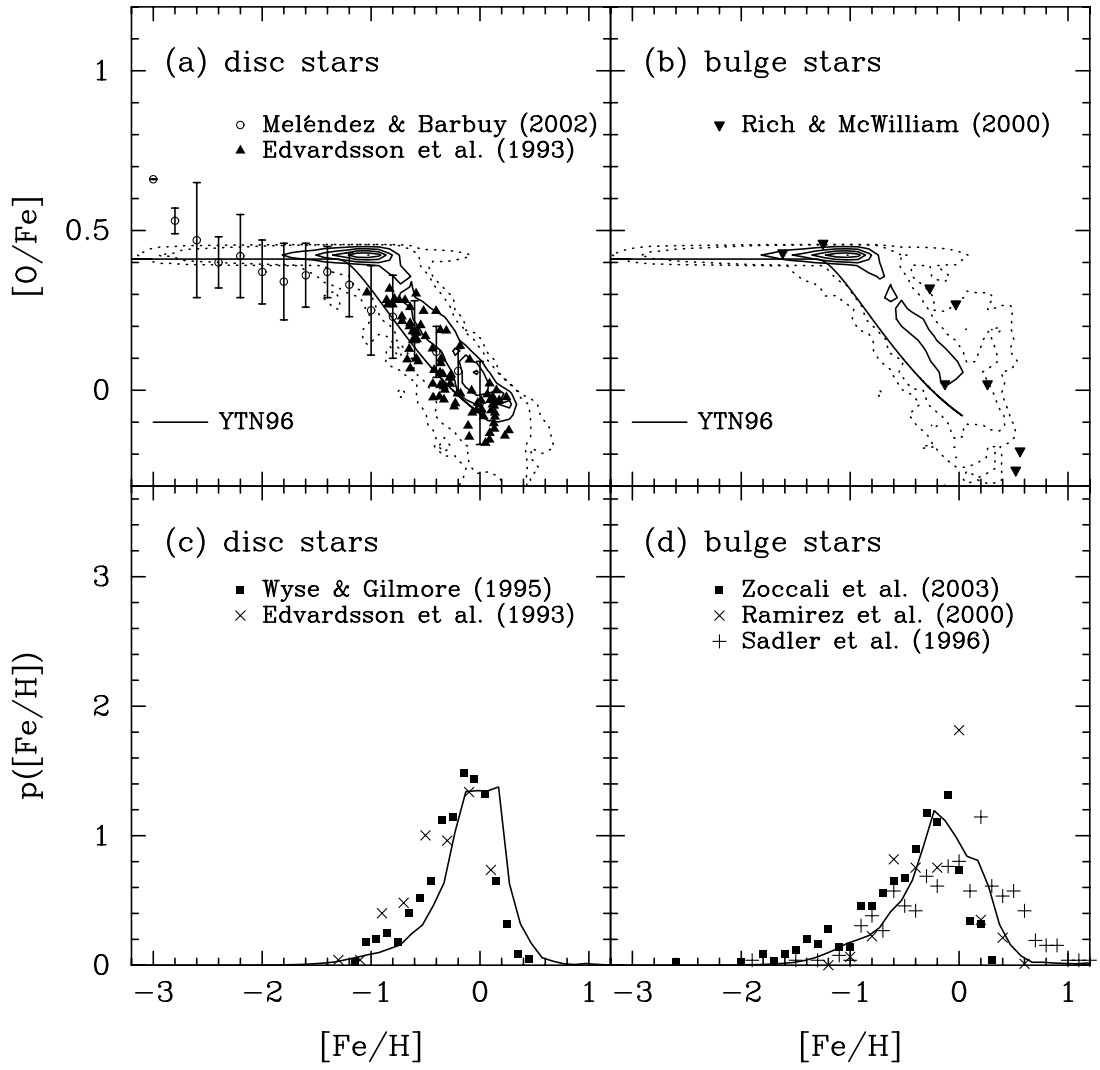

FIG. 17.—Same as Fig. 3, but for $V_{hot} = 70$ km s^{-1}. [*See the electronic edition of the Journal for a color version of this figure.*]

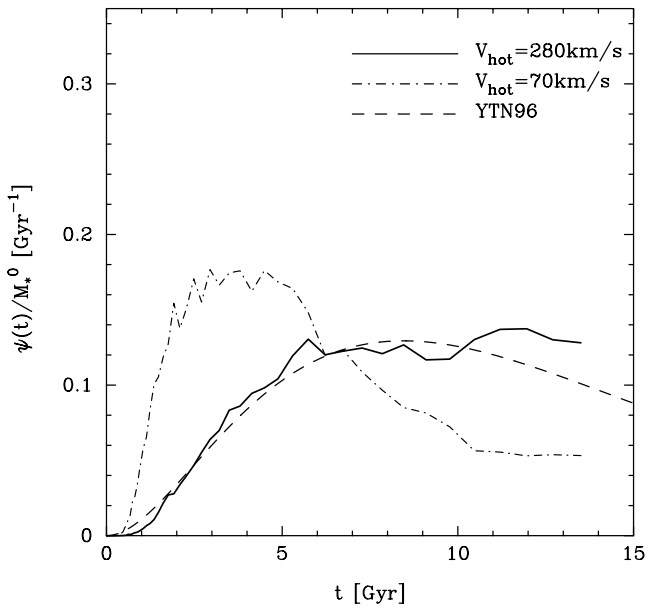

FIG. 18.—Star formation histories. The solid and dot-dashed lines indicate models with $V_{hot} = 280$ and 70 km s^{-1}, respectively. The dashed line denotes the infall model. [*See the electronic edition of the Journal for a color version of this figure.*]

but they are not a dominant fraction. Increasing observational data will provide a strong constraint on bulge formation.

As a by-product, we have obtained the luminosity function of galaxies in Local Group halos. Recent high-resolution *N*-body simulations have predicted many more dwarf-scale dark halos than observed satellite galaxies, and this has been considered to be a serious problem (Klypin et al. 1999; Moore et al. 1999). Such an overabundance problem has been solved in the framework of the SA models taking into account effects of reionization and incompleteness due to significantly low surface brightness (Somerville 2002; Benson et al. 2002a). Our model also shows an ability to solve this problem in a similar manner to those works.

The chemical yields we used are the same as those in Yoshii et al. (1996), in which an infall model of monolithic collapse was used (Arimoto et al. 1992). The similarity between our hierarchical model and the monolithic cloud collapse model suggests that spiral galaxies in a hierarchical universe should have a similar formation history to that modeled by the monolithic cloud collapse model, as shown in Baugh et al. (1996). The star formation histories we computed also suggest these similarities. However, this does not always mean that similar star formation histories provide similar chemical enrichment histories. As shown in § 7.3 and more directly by equation (11), SN feedback plays a critical role in chemical enrichment.

In this paper we have concentrated on investigating the [O/Fe] relation and the [Fe/H] distribution. Since recent analyses of solar neighborhood stars have revealed that the age-metallicity relation has a large scatter, it will be useful as a next step to see whether our model can reproduce this relation as well as the scatter in it (Ibukiyama & Arimoto 2002). Furthermore, while the analysis in this paper focused only on MW-like galaxies, our SA model has the potential ability to investigate other systems simultaneously. Investigating abundance ratios in such systems as the intracluster medium, the stars composing elliptical galaxies, and damped Lyα systems will provide independent, important clues to understanding galaxy formation. The cosmic explosion rate of SNe Ia will also give a new insight into both galaxy formation and observational cosmology. We will pursue these topics in future papers.

We would like to thank Takuji Tsujimoto for useful suggestions and Cedric G. Lacey for reading our paper carefully. We also acknowledge support from the PPARC rolling grant for extragalactic astronomy and cosmology at Durham and from the Japan Society for the Promotion of Science for Young Scientists (00207 and 01891).

REFERENCES

Arimoto, N., & Yoshii, Y. 1986, A&A, 164, 260
———. 1987, A&A, 173, 23
Arimoto, N., Yoshii, Y., & Takahara, F. 1992, A&A, 253, 21
Baugh, C. M., Cole, S., & Frenk, C. S. 1996, MNRAS, 283, 1361
Baugh, C. M., Lacey, C. G., Frenk, C. S., Granato, G. L., Silva, L., Bressan, A., Benson, A. J., & Cole, S. 2005, MNRAS, 356, 1191
Benson, A. J., Frenk, C. S., Baugh, C. M., Cole, S., & Lacey, C. G. 2003, MNRAS, 343, 679
Benson, A. J., Frenk, C. S., Lacey, C. G., Baugh, C. M., & Cole, S. 2002a, MNRAS, 333, 177
Benson, A. J., Lacey, C. G., Baugh, C. M., Cole, S., & Frenk, C. S. 2002b, MNRAS, 333, 156
Berczik, P. 1999, A&A, 348, 371
Binney, J., & Tremaine, S. 1987, Galactic Dynamics (Princeton: Princeton Univ. Press)
Chiappini, C., Matteucci, F., & Gratton, R. 1997, ApJ, 477, 765
Cole, S., Aragon-Salamanca, A., Frenk, C. S., Navarro, J. F., & Zepf, S. E. 1994, MNRAS, 271, 781
Cole, S., Lacey, C. G., Baugh, C. M., & Frenk, C. S. 2000, MNRAS, 319, 168
Edvardsson, B., Andersen, J., Gustafsson, B., Lambert, D. L., Nissen, P. E., & Tomkin, J. 1993, A&A, 275, 101
Fenner, Y., & Gibson, B. K. 2003, Publ. Astron. Soc. Australia, 20, 189
Gal-Yam, A., & Maoz, D. 2004, MNRAS, 347, 942
Greggio, L., & Renzini, A. 1983, A&A, 118, 217
Ibukiyama, A., & Arimoto, N. 2002, A&A, 394, 927
Ishimaru, Y., & Wanajo, S. 1999, ApJ, 511, L33
Kauffmann, G. 1996, MNRAS, 281, 475
Kauffmann, G., & Charlot, S. 1998, MNRAS, 294, 705
Kauffmann, G., White, S. D. M., & Guiderdoni, B. 1993, MNRAS, 264, 201
Kawata, D. 2001, ApJ, 558, 598
Kawata, D., & Gibson, B. K. 2003a, MNRAS, 340, 908
———. 2003b, MNRAS, 346, 135
Kennicutt, R. C. 1983, ApJ, 272, 54
Klypin, A. A., Kravtsov, A. V., Valenzuela, O., & Prada, F. 1999, ApJ, 522, 82
Kobayashi, C. 2004, MNRAS, 347, 740
Kobayashi, C., Tsujimoto, T., Nomoto, K., Hachisu, I., & Kato, M. 1998, ApJ, 503, L155
Kodama, T., & Arimoto, N. 1997, A&A, 320, 41
Lacey, C. G., & Fall, S. M. 1983, MNRAS, 204, 791
———. 1985, ApJ, 290, 154
Lia, C., Portinari, L., & Carraro, G. 2002, MNRAS, 330, 821
Maciel, W. J. 2001, NewA Rev., 45, 571
Makino, J., & Hut, P. 1997, ApJ, 481, 83
Martin, N. F., Ibata, R. A., Bellazzini, M., Irwin, M. J., Lewis, G. F., & Dehnen, W. 2004, MNRAS, 348, 12
Mateo, M. L. 1998, ARA&A, 36, 435
Matteucci, F., & Brocato, E. 1990, ApJ, 365, 539
Matteucci, F., & François, P. 1989, MNRAS, 239, 885
Matteucci, F., & Greggio, L. 1986, A&A, 154, 279
McWilliam, A., Rich, R. M., & Smecker-Hane, T. A. 2003, ApJ, 592, L21
Meléndez, J., & Barbuy, B. 2002, ApJ, 575, 474
Moore, B., Ghigna, S., Governato, F., Lake, G., Quinn, T., Stadel, J., & Tozzi, P. 1999, ApJ, 524, L19
Nagashima, M., & Gouda, N. 2001, MNRAS, 325, L13
Nagashima, M., Gouda, N., & Sugiura, N. 1999, MNRAS, 305, 449
Nagashima, M., Lacey, C. G., Baugh, C. M., Frenk, C. S., & Cole, S. 2005a, MNRAS, 358, 1247
Nagashima, M., Lacey, C. G., Okamoto, T., Baugh, C. M., Frenk, C. S., & Cole, S. 2005b, MNRAS, 363, L31
Nagashima, M., Totani, T., Gouda, N., & Yoshii, Y. 2001, ApJ, 557, 505
Nagashima, M., & Yoshii, Y. 2003, MNRAS, 340, 509
———. 2004, ApJ, 610, 23
Nagashima, M., Yoshii, Y., Totani, T., & Gouda, N. 2002, ApJ, 578, 675
Nakasato, N., & Nomoto, K. 2003, ApJ, 588, 842
Nordström, B., et al. 2004, A&A, 418, 989
Okamoto, T., Eke, V. R., Frenk, C. S., & Jenkins, A. 2005, MNRAS, 363, 1299
Okamoto, T., Jenkins, A., Eke, V. R., Quilis, V., & Frenk, C. S. 2003, MNRAS, 345, 429
Okoshi, K., Nagashima, M., Gouda, N., & Yoshioka, S. 2004, ApJ, 603, 12
Pagel, B. E. J., & Patchett, B. E. 1975, MNRAS, 172, 13
Pagel, B. E. J., & Tautvaišienė, G. 1995, MNRAS, 276, 505
Raiteri, C. M., Villata, M., & Navarro, J. F. 1996, A&A, 315, 105
Ramírez, S. V., Stephens, A. W., Frogel, J. A., & DePoy, D. L. 2000, AJ, 120, 833
Rich, R. M., & McWilliam, A. 2000, Proc. SPIE, 4005, 150
Sadler, E. M., Rich, R. M., & Terndrup, D. M. 1996, AJ, 112, 171
Salpeter, E. E. 1955, ApJ, 121, 161
Schmidt, M. 1963, ApJ, 137, 758
Somerville, R. S. 2002, ApJ, 572, L23
Somerville, R. S., & Kolatt, T. 1999, MNRAS, 305, 1
Somerville, R. S., & Primack, J. R. 1999, MNRAS, 310, 1087
Somerville, R. S., Primack, J. R., & Faber, S. M. 2001, MNRAS, 320, 504
Sugiyama, N. 1995, ApJS, 100, 281
Sutherland, R., & Dopita, M. A. 1993, ApJS, 88, 253
Thomas, D. 1999, MNRAS, 306, 655
Thomas, D., & Kauffmann, G. 1999, in ASP Conf. Ser. 192, Spectrophotometric Dating of Stars and Galaxies, ed. I. Hubeny, S. Heap, & R. Cornett (San Francisco: ASP), 261
Tinsley, B. M. 1980, Fundam. Cosmic Phys., 5, 287
Tsujimoto, T., Nomoto, K., Yoshii, Y., Hashimoto, M., Yanagida, Y., & Thielemann, F.-K. 1995, MNRAS, 277, 945
Tsujimoto, T., Shigeyama, T., & Yoshii, Y. 1999, ApJ, 519, L63
van den Bergh, S. 1962, AJ, 67, 486
Wyse, R. F. G., & Gilmore, G. 1995, AJ, 110, 2771
Yoshii, Y., Tsujimoto, T., & Nomoto, K. 1996, ApJ, 462, 266
Zoccali, M., et al. 2003, A&A, 399, 931